UNIVERSITY OF CALIFORNIA

SANTA CRUZ

THE EFFECT OF SINGLE-CELL KNOCKOUT OF FRAGILE X MESSENGER RIBONUCLEOPROTEIN ON STRUCTURAL SYNAPTIC PLASTICITY

A thesis submitted in partial satisfaction
of the requirements for the degree of

MASTER OF SCIENCE

in

MOLECULAR, CELL AND DEVELOPMENTAL BIOLOGY

by

Marie Gredell

June 2023

The Thesis of Marie Gredell
is approved:

_____
Professor Yi Zuo, Chair

_____
Professor Bin Chen

_____
Professor Euiseok Kim

_____
Peter Biehl
Vice Provost and Dean of Graduate Studies

Table of Contents

List of Figures

ABSTRACT

Marie Gredell

The Effect of Single-Cell Knockout of Fragile X Messenger Ribonucleoprotein on Structural Synaptic Plasticity

The Fragile X Syndrome (FXS), the most common inherited intellectual disability, is caused by a loss-of-function mutation in the *FMR1* gene encoding the Fragile X Messenger Ribonucleoprotein (FMRP). The morphological hallmark of FXS in humans and *Fmr1* knockout (KO) mice is an abnormally high density and immature morphology of dendritic spines on cortical pyramidal neurons (PyrNs). To determine whether this phenotype arises cell-autonomously from the lack of FMRP, we sparsely deleted FMRP from layer 5 PyrNs and imaged these cells *in vivo* in adolescence and adulthood. We found that single-cell *Fmr1* KO in adulthood does not affect spine density, morphology, or dynamics, but neonatal *Fmr1* KO leads to normal spine density yet elevated spine formation at 1 month of age. These data reveal cell-autonomous FMRP regulation of cortical synaptic dynamics during adolescence, but spine defects in adulthood also implicate non-cell-autonomous factors.

To my family, friends, and animals used in this study.

I couldn't have done this without you.

ACKNOWLEDGEMENTS

First and foremost, I would like to thank my advisor and mentor Dr. Yi Zuo for the incredible learning experience of working in her research lab. Yi's dedication to scientific discovery and endless passion for learning is unmatched and such an inspiration. She has been not only a great mentor for my research but also in career exploration and life as a whole. Her excitement for science is infectious—I would leave weekly meetings with her feeling unstoppable and motivated to give my projects my all. I am so fortunate and grateful to have had this opportunity to work so closely with her.

I would also like to thank Dr. Ju Lu for his mentorship both in my undergraduate and graduate career. He taught me everything I know about conducting neuroscience research and is a remarkable source of knowledge not only for neuroscience but physics, microscopy, writing and more. He was instrumental in helping me publish this research and it's been such an honor working with him. I am so appreciative that he took a chance on me as an undergrad and encouraged me to stay at UCSC for a Master's.

I am incredibly grateful to my committee members, Dr. Bin Chen and Dr. Euiseok Kim, for all of their support and encouragement on my project. Discussing experiments to continue this project and their feedback and questions during my presentations have helped me grow as both a researcher and communicator. I am honored that they have given their time to me to serve on my committee.

All of the members of the Zuo lab have inspired me and helped me grow so much as a scientist. I would like to thank Jacob Baker for our insightful scientific conversations and for rooting for my success and happiness in the Zuo lab and in my career beyond my time at UCSC. His high-fives on his way in and out of the lab always boosted my mood. I would also like to thank Shaorong Ma and Hyo Gun Lee for inspiring me with their drive and palpable enthusiasm for neuroscience research. They are incredible scientists, and I am fortunate to have worked alongside them. I would also like to thank Stefan Abreo for the camaraderie, and all of the lab's undergraduates for keeping me in touch with the undergraduate experience at UCSC. Lastly, I would like to thank Ines Erkizia-Santamaría for quickly becoming my closest friend in the Zuo lab even with her international rotation being so short. Her professional and personal support have meant the world to me, and I hope our paths cross again in the near future.

I have been fortunate to have had the best cohort when I joined this program. I will forever cherish the friendships and time I spent with everyone, but specifically Josie Bleeker, Cole R. K. Harder, Natalie Pedicino, Chloe Wohlenberg, Shally Saini, and Silvart Larine. All of them have helped me come into my own as a scientist at UCSC and I can't wait to see all they accomplish in the years to come.

I would like to thank the incredible friends that have supported me in many ways throughout this journey: Sarah Adamson, Kayleigh Boyd, Daisy Cortes, Gabby Nobili, Bailey Zazueta, Levi Matsushima, Chris Condon, Lily Karim, Caison Warner, Allyson McAtamney, Kaitlyn Gomez, Riley Blue, Shanna Howard, Zia Flaminio,

Usaamah Saeed, Mikey Dang and Nick Ball-Jones. The wonderful times with you all have been the highlight of my time here.

Most of all, I would like to give my thanks to my family. I would never have had the courage to dip my feet into neuroscience research if it weren't for my dad and stepmom, Gary Gredell and Julie Oseland. Their unconditional love and support have been the biggest blessing of my life. Words cannot describe how much they mean to me, and I can't thank them enough for their endless support. I would also like to thank my brother, Matthew Gredell, for being my rock and listening to all of my daily recaps. His constant support and desire for me to be my happiest self have helped me immensely throughout this program. I also thank my stepsisters, Sarah and Leah Tannehill, for being inspirations and role models to me. I have so much love for all of you.

CHAPTER 1: INTRODUCTION

The text of this thesis includes a reprint of the following previously published material: Gredell, M., Lu, J. & Zuo, Y. 2023. The Effect of Single-Cell Knockout of Fragile X Messenger Ribonucleoprotein on Synaptic Structural Plasticity. *Frontiers in Synaptic Neuroscience,* 15:1135479. The co-authors listed in this publication directed and supervised the research which forms the basis for the thesis.

1.1 The Fragile X Syndrome (FXS)

The Fragile X syndrome (FXS) is the most common inherited intellectual disorder, affecting roughly 1 in 7,000 males and 1 in 11,000 females in the overall population according to a recent meta-analysis (Hunter, Rivero-Arias et al. 2014). FXS is characterized by a variety of physical, behavioral, and cognitive symptoms (Berry-Kravis 2002;Turk 2011). Common physical characteristics of FXS patients include an elongated forehead, hypermobile joints, macroorchidism, and, in more severe cases, seizures. FXS behavioral phenotypes include repetitive speech and echolalia, hyperacusis, repetitive movements, social anxiety, and aversion to eye contact; its cognitive symptoms include impaired working memory, information processing, arousal modulation, and executive function.

FXS is caused by the expansion of a CGG trinucleotide repeat in the *FMR1* gene on the X chromosome (Verkerk, Pieretti et al. 1991). Healthy individuals possess between 5 and 44 CGG repeats in the *FMR1* gene. Those with more than 200 repeats are considered as having the full mutation (FM); those with alleles possessing

between 55 and 200 repeats are considered premutation, as the likelihood of expansion due to instability, and thus the potential to give rise to affected offspring, is significantly increased (Maddalena, Richards et al. 2001). Premutation individuals also interestingly exhibit symptoms of FXS to a milder extent, including some impairments in social behavior and learning (Turk 2011).

The FM expansion results in the methylation of a CpG island in the *FMR1* promoter, resulting in transcriptional silencing of the *FMR1* gene (Pieretti, Zhang et al. 1991;Vincent, Heitz et al. 1991). The molecular mechanisms underlying this recognition of the FM expansion and concomitant methylation of the *FMR1* promoter region remain to be elucidated.

1.2 Mouse Models of FXS

The mouse has been heavily used in biomedical research as a model organism for its short gestational period, fast development, genome similarity to humans, and ease of housing, breeding, and genetic manipulation. The murine *Fmr1* gene shares 97% homology with human *FMR1* (Ashley, Sutcliffe et al. 1993), making the mouse an ideal model organism for studying FXS. To replicate the human FXS condition, researchers first attempted to generate an *Fmr1* knock-in mouse line by utilizing the genetic instability of *Fmr1* premutation alleles. Fertilized eggs were microinjected with a CGG-expanded *Fmr1* gene, and in adulthood, these mice were mated in hopes of producing offspring with increased CGG repeats. Mice with 81, 88 and 120 repeats all failed to produce offspring with large CGG expansions, a surprising result as

repeats of these lengths in humans are highly unstable and very likely to expand (Bontekoe, de Graaff et al. 1997;Lavedan, Garrett et al. 1997;Lavedan, Grabczyk et al. 1998). The mouse *Fmr1* gene begins to become unstable and more likely to expand as the number of repeats approaches 200. However, in mice with up to 230 CGG repeats, FMRP remains expressed (though at a reduced level), and the upstream promoter sequence is not hypermethylated (Entezam, Biacsi et al. 2007).

As the knock-in mouse only mimics the human premutation condition, efforts turned to a full *Fmr1* knockout (KO) model of FXS. The *Fmr1* global KO mouse generated over three decades ago (The Dutch-Belgian Fragile X Consortium, 1994) exhibits a variety of behavioral and neurological phenotypes comparable to the human condition (Wisniewski, Segan et al. 1991;Musumeci, Hagerman et al. 1999;Rais, Binder et al. 2018). For example, male *Fmr1* global KO mice have defective social behaviors: they show a decreased preference to novel social stimulus, decreased time spent in affiliative behaviors with female mice, and increased self-grooming when a female mouse is present (Pietropaolo, Guilleminot et al. 2011). They also exhibit heightened perseveration, responding, and hyperactivity during novel rule acquisition and during exposure to novel environments (Kramvis, Mansvelder et al. 2013), and impaired memory encoding in fear conditioning (Li, Jiang et al. 2020). Susceptibility to audiogenic seizures are also increased in *Fmr1* global KO mice (Musumeci, Bosco et al. 2000). Taken together, these findings validate the *Fmr1* global KO mouse as a model of FXS.

In addition to the global KO mouse model, an *Fmr1* conditional knockout (CKO) mouse line has been created (Mientjes, Nieuwenhuizen et al. 2006). This line has the promoter and the first exon of the *Fmr1* gene flanked by bacteriophage-derived loxP sites, thus allowing for Cre recombinase-induced recombination and subsequent deletion of the gene. Many studies have utilized this CKO mouse to examine FMRP function in specific cell types, including forebrain excitatory neurons (Lovelace, Rais et al. 2020), parvalbumin interneurons (Kalinowska, van der Lei et al. 2022), inferior colliculus glutamatergic neurons (Gonzalez, Tomasek et al. 2019), granule cells in the dentate gyrus (Monday, Kharod et al. 2022), pyramidal neurons in the primary somatosensory cortex (Zhang, Gibson et al. 2021), and astrocytes (Higashimori, Schin et al. 2016;Hodges, Yu et al. 2017;Jin, Higashimori et al. 2021), either by crossing *Fmr1* CKO mice with a suitable Cre-expressing driver line, or by injecting Cre-encoding viruses.

1.3 The Fragile X Messenger Ribonucleoprotein (FMRP)

The Fragile X Messenger Ribonucleoprotein (FMRP), which is encoded by the *Fmr1* gene, is predominantly expressed in the brain and testes in both humans and mice, with lower expression in the placenta, lung, and kidney (Hinds, Ashley et al. 1993). In the brain, FMRP is found in both neurons and glial cells, and is predominantly cytoplasmic (Giampetruzzi, Carson et al. 2013;Richter and Zhao 2021). FMRP is present in dendrites and dendritic spines, postsynaptic sites important for the induction and maintenance of synaptic plasticity. *Fmr1* mRNA is locally

translated in an activity-dependent manner, producing FMRP at dendritic spines in response to the activation of metabotropic glutamate receptors (mGluRs) (Weiler, Irwin et al. 1997;Antar, Afroz et al. 2004;Ferrari, Mercaldo et al. 2007).

FMRP is involved in regulating almost all aspects of gene expression (Richter and Zhao 2021). It is particularly critical for the transportation and local translation of mRNAs that regulate dendritic growth, synaptic development, and plasticity (Bassell and Warren 2008). As an RNA-binding protein, FMRP interacts with mRNAs encoding many pre- and postsynaptic proteins, resulting in ribosome stalling during translation and thus repressing the expression of the protein products (Darnell, Van Driesche et al. 2011). It has been shown that FMRP interacts with the mRNAs of neuroligin, MAP1B, CaMKII, and PSD-95, all of which play roles in synapse development and maintenance (Muddashetty, Kelic et al. 2007;Menon, Mader et al. 2008;Chmielewska, Kuzniewska et al. 2019).

1.4 Dendritic Spine Plasticity and Morphology in FXS

Postmortem examination has revealed that the neuronal morphological hallmark of FXS is a higher overall density of dendritic spines, and particularly a higher density of long and thin dendritic spines, on cortical neurons (Rudelli, Brown et al. 1985;Hinton, Brown et al. 1991;Irwin, Patel et al. 2001;Beckel-Mitchener and Greenough 2004). These phenotypes were found on apical dendrites of pyramidal neurons in the parieto-occipital neocortex (Rudelli, Brown et al. 1985;Hinton, Brown et al. 1991), as well as on basal dendrites in temporal and visual cortices (Irwin, Patel

et al. 2001) of human patients. *Fmr1* global KO mice also display similarly increased spine density, as well as a higher percentage of immature-appearing (long, thin, and tortuous) spines, on apical dendrites of L5 pyramidal cells in occipital, visual, and somatosensory cortices, as well as on pyramidal neurons in hippocampal CA1 region (Comery, Harris et al. 1997;Irwin, Idupulapati et al. 2002;Galvez and Greenough 2005;McKinney, Grossman et al. 2005;Grossman, Elisseou et al. 2006).

The morphology of a dendritic spine is directly related to its physiological function, with both neck and head size playing roles in synaptic transmission. Dendritic spines with longer necks have a shorter latency and slower decay kinetics of calcium responses (Hering and Sheng 2001). The volume of the spine head also directly correlates with the number of α-amino-3-hydroxy-5-methyl-4-isoxazolepropionic acid (AMPA) receptors (Matsuzaki, Ellis-Davies et al. 2001), which mediate most of the fast excitatory glutamatergic neurotransmission in the central nervous system (Diering and Huganir 2018). Thus, the abnormal spine morphology in FXS may alter how the neuron responds to presynaptic inputs and ultimately how the neural circuit functions.

In addition to altered spine morphology and density, *Fmr1* global KO mice have altered structural dynamics (formation and elimination) of spines in an age-, region-, and cell type-specific manner (Cruz-Martín, Crespo et al. 2010;Pan, Aldridge et al. 2010;Padmashri, Reiner et al. 2013;Hodges, Yu et al. 2017). Previous studies have found that the rate of dendritic spine formation increases throughout the cortex in *Fmr1* KO adolescent mice; reports on spine elimination rate in these mice are

somewhat inconsistent, with some studies showing elevated spine elimination compared to WT animals and others reporting no difference (Cruz-Martín, Crespo et al. 2010;Pan, Aldridge et al. 2010;Padmashri, Reiner et al. 2013;Hodges, Yu et al. 2017). The excess of spine formation relative to spine elimination during adolescence would explain the elevated spine density seen in adulthood (Hodges, Yu et al. 2017;Arroyo, Fiole et al. 2019;Bland, Aharon et al. 2021).

1.5 Circuit Defects in FXS

Previous studies have shown that *Fmr1* global KO mice have abnormal neuronal activity pattern and synchronization in the neocortex and the hippocampus (Gibson, Bartley et al. 2008;Hays, Huber et al. 2011;Paluszkiewicz, Olmos-Serrano et al. 2011;Arbab, Battaglia et al. 2018;Scharkowski, Frotscher et al. 2018;Cheyne, Zabouri et al. 2019). Such functional abnormalities may have profound impacts on the synaptic circuit. It is well recognized that many intracellular signaling pathways that regulate spine formation and maturation are activity-dependent (Saneyoshi, Fortin et al. 2010). Long-term potentiation (LTP), which strengthens synaptic connections, has been shown to be reduced in cortical, but not hippocampal, neurons of *Fmr1* global KO mice (Li, Pelletier et al. 2002). The LTP deficit may manifest itself in the elevated density of immature-appearing dendritic spines in the cortex. As spine elimination has been associated with activity-dependent processes such as long-term depression (LTD) and competition between active and inactive neighboring synapses (Stein and Zito 2019), these plasticity mechanisms may translate the

anomalous neuronal activities into defective structural plasticity of synapses. Interestingly, in the somatosensory cortex of *Fmr1* global KO mice, local excitatory drive to fast-spiking inhibitory interneurons is dramatically decreased, and the intrinsic membrane excitability of excitatory neurons is increased (Gibson, Bartley et al. 2008). All these alterations result in an overall hyperexcitability of cortical circuits, which may ultimately underlie the cognitive deficits associated with FXS.

Such complex interplay between cellular and network-level mechanisms raises an interesting question: is the alteration in FXS spine structure and dynamics the result of cell-autonomous dysregulation, or of abnormal activities in the neuronal network?

CHAPTER 2: METHODS

2.1 Experimental Animals

The *Fmr1* global KO mouse line (JAX #003025) was obtained from Dr. Stephen T. Warren's lab at Emory University; the *Fmr1* CKO mouse line (Mientjes, Nieuwenhuizen et al. 2006) was obtained from Dr. David L. Nelson's lab at Baylor College of Medicine; the Thy1-GFP-M (JAX #007788) mouse line was obtained from The Jackson Laboratory. All mice have been maintained in the C57BL6/J (JAX #000664) background for many generations. Mice were group-housed with littermates and maintained on a 12 h light/dark cycle. All animal experiments were carried out in accordance with protocols approved by The Institutional Animal Care and Use Committee of University of California, Santa Cruz. Only male mice were used for experiments.

2.2 Virus Injection and Cranial Window Implantation in Adult Mice

Virus injection and cranial window implantation in adult mice (6-8 weeks old) were performed as described previously (Lu, Tjia et al. 2021). Briefly, the mouse was anesthetized with isoflurane in oxygen (4% for induction and 1.5% for maintenance), then placed on the stereotaxic frame. Ophthalmic ointment was applied to the eyes to prevent desiccation and irritation. Carprofen (5 mg/kg bodyweight, intraperitoneal), buprenorphine (0.1 mg/kg, subcutaneous), enrofloxacin (5 mg/kg, subcutaneous), and dexamethasone (2 mg/kg, intramuscular) were administered. The fur on the top of the head was removed with a blade; the exposed scalp was sterilized with betadine

followed by 70% alcohol. A midline scalp incision was made, and the periosteum was gently scraped off from the skull. A circular piece of the skull (centered at AP = -1 mm, ML = 1.5 mm) was removed with a trephine (diameter = 2.3 mm, Fine Science Tools, Foster City, CA) driven by a high-speed micro-drill (Foredom K1070, Blackstone Industries, LLC, Bethal, CT). AAV2/1-hSyn-Cre virus (Addgene 105553-AAV1, $2.6x10^{13}$ gc/ml) or AAV2/1-CaMKII0.4-Cre-SV40 virus (U Penn Vector Core, $2.94x10^{13}$ gc/ml) was diluted 1:5,000 in sterile saline and then mixed in a 1:1 ratio with AAV2/1-CAG-Flex-EGFP (Addgene 51502-AAV1, $2.96x10^{13}$ gc/ml). 100 nl of the virus mixture was injected into the center of the window at a depth of 0.6 mm from the cortical surface at a rate of 20 nl/min using a custom-made injection system based on a single-axis oil hydraulic micromanipulator (MO-10, Narishige, Tokyo, Japan). The imaging port was made by gluing a circular cover glass (#2, diameter = 2.2 mm) underneath a doughnut-shaped glass (#1, inner diameter = 2 mm, outer diameter = 3 mm; Potomac Photonics, Inc., Baltimore, MD). The imaging port was mounted so that the bottom cover glass fit snugly into the cranial window and the top glass doughnut rested above the skull. The imaging port was secured with a UV-cured adhesive (Fusion Flo, Prevest DenPro, Jammu, India) onto the skull. After the solidification of the adhesive, the scalp flaps were closed with suture. Following two weeks of recovery and virus incubation, the central piece of the scalp was excised, and a custom-made stainless-steel head-bar was secured over the skull with dental cement (Jet Denture Repair, Lang Dental, Wheeling, IL). The mouse received

enrofloxacin, buprenorphine, and dexamethasone once per day for two extra days post-surgery and was allowed to recover for an additional week prior to imaging.

2.3 *In vivo* Imaging of Dendritic Spines through the Cranial Window

In vivo imaging of dendritic spines through the cranial window was performed on a two-photon microscope (Ultima Investigator, Bruker Co., Middleton, WI) using a 16x/0.8 NA water-immersion objective (Nikon Instruments, Inc., Melville, NY) and an ultrafast two-photon laser (Mai Tai, Spectra-Physics, Santa Clara, CA) operating at 940 nm wavelength. The mouse was anesthetized with a mixture of ketamine (20 mg/ml) and xylazine (2.0 mg/ml) in 0.9% sterile saline administered intraperitoneally (5 ml/kg bodyweight). It was then placed onto a custom-made holding stage, secured by the head-bar. Prior to the first imaging session, images of blood vessels were taken under a dissection microscope as a reference for subsequent relocations. Stacks of two-photon images were taken at 12x zoom with a z-step size of 1 μm. After the first imaging session, low-magnification image stacks (1x and 4x zoom, z-step size = 3 μm) were taken to facilitate relocation.

2.4 Virus Injection in Neonatal Mice

Virus injection in neonatal mice was performed as previously described (Chen, Lu et al. 2018). Briefly, the postnatal (P) day 1-3 mouse was cryo-anesthetized by placement on ice. AAV2/1-CaMKII0.4-Cre-SV40 (U Penn Vector Core, 2.94×10^{13} gc/ml) was diluted 1:5000 in sterile saline and then mixed in a 1:1 ratio

with AAV2/1-CAG-Flex-EGFP (Addgene 51502-AAV1, 2.96×10^{13} gc/ml). 100 nl of the virus mixture was injected at a rate of 40 nl/min into the primary somatosensory cortex (AP = 1.75 mm from lambda, ML = 1.25 mm; depth = 0.35 mm) through the scalp and the skull. 4 weeks of incubation were allowed before imaging and immunohistochemical experiments.

2.5 Thin Skull Preparation for *In Vivo* Imaging of Dendritic Spines

The thin skull procedure was performed on young (1-month old) mice as previously described (Xu, Yu et al. 2009). Briefly, the mouse was anesthetized with a mixture of ketamine (20 mg/ml) and xylazine (2.0 mg/ml) in 0.9% sterile saline administered intraperitoneally (5 ml/kg body weight). Ophthalmic ointment was applied to the eyes to prevent desiccation and irritation, and the fur over the scalp was removed with a blade. A midline incision was made through the scalp and the periosteum was gently scraped off from the skull. A high-speed micro-drill (Foredom K1070, Blackstone Industries, LLC, Bethal, CT) and a microblade were used to thin a small region of the skull to ~20 μm thickness. A custom-made head-plate with a central opening was attached to the skull by cyanoacrylate glue (Krazy Glue, Elmer's Products, Westerville, OH), centered over the thinned region. The head-plate was secured onto a custom-made metal baseplate to stabilize the mouse's head during imaging. Two-photon imaging was performed as described above. After imaging, the head-plate was detached from the skull, the skull was cleaned with sterile saline, and the scalp was sutured.

2.6 Dendritic Spine Data Analysis

Images were analyzed using ImageJ as described previously (Xu, Yu et al. 2009). A spine was considered eliminated if it was present in the initial image but not in the subsequent image. A spine was considered to have newly formed if it was not present in the initial image but present in the subsequent image. The percentage of spines eliminated/formed was calculated as the number of spines eliminated/formed over the total spines counted from the first imaging session. Spine density was measured by dividing the number of spines on a dendritic segment by the length of the segment. Spines were classified into four morphological categories (mushroom, stubby, thin, and other) as previously described (Hodges, Yu et al. 2017).

2.7 Immunohistochemistry

The mouse was transcardially perfused with 4% paraformaldehyde (PFA) in 0.01M phosphate buffered saline (PBS). The brain was removed and post-fixed in 4% PFA overnight at 4°C. For all experiments, the brain was cut into 40 μm sections using a vibratome (VT1000S, Leica Biosystems, Deer Park, IL). Sections were permeabilized and blocked with 0.5% Triton X-100 and 10% normal goat serum in PBS, then incubated with rabbit anti-FMRP (1:1,000; Sigma-Aldrich, F4055) and mouse anti-NeuN (1:1,000; Millipore, MAB377) in 0.5% Triton X-100 in PBS at 4°C overnight. Sections were then incubated with goat anti-rabbit secondary antibody conjugated to Alexa Fluor 594 (1:1,000; Life Technologies, A11037) and goat anti-mouse secondary antibody conjugated to Alexa Fluor 647 (1:1,000; Life

Technologies, A21235) in 10% normal goat serum in PBS for 2 h at room temperature. After rinsing in PBS, sections were incubated in 4′,6-diamidino-2-phenylindole (DAPI, 1:36,000) for 15 min. Sections were then mounted with Fluoromount-G mounting medium (Cat# 0100-01, SouthernBiotech, Birmingham, AL). Images were captured with a Zeiss Axiolmager Z2 widefield fluorescence microscope using a 2.5x/0.12 NA or 10x/0.45 NA, or with a Zeiss 880 confocal microscope using a 20x/0.8 NA air objective. The density of neurons with GFP, FMRP, or NeuN labeling was quantified using Neurolucida Explorer 11 (MBF Bioscience, Williston, VT). Individual cells were analyzed for the presence of GFP, FMRP, and NeuN.

2.8 Statistical Analysis

Statistical analyses were performed using GraphPad Prism 9.3.1. The Shapiro–Wilk test was used to test for normality. If samples passed the normality test, Student's t-test was used for two-sample comparison; otherwise Mann-Whitney test was used. For multi-sample comparison, one-way or two-way ANOVA was used, followed by post hoc Dunnett's or Šidák test (compared with the control group). The sample difference was considered significant if $p < 0.05$. Data are presented as mean ± s.e.m.

CHAPTER 3: RESULTS

3.1 Single-cell FMRP knockout (KO) strategy

To investigate whether FMRP regulates the structural plasticity of synapses cell-autonomously, we knocked out FMRP from a sparse subset of L5 PyrNs in the primary somatosensory cortex (S1) of *Fmr1* CKO mice. We chose to target S1 because previous studies have revealed altered tactile information processing (Juczewski, von Richthofen et al. 2016;He, Cantu et al. 2017) and abnormal dendritic spine development (Galvez and Greenough 2005;Till, Wijetunge et al. 2012) in this area of adult *Fmr1* global KO ("GKO") mice. We accomplished this by injecting a mixture of highly diluted adeno-associated virus (AAV) encoding the Cre recombinase and another AAV encoding floxed green fluorescent protein (GFP) into S1 of CKO mice (Figure 1A). This strategy removes the promoter region and the first exon of the *Fmr1* gene via Cre-dependent recombination, thus preventing *Fmr1* transcription. At the same time, the Cre-dependent GFP expression allows us to visualize the cells in which *Fmr1* has been knocked out and enables analysis of dendrites and dendritic spines (Figure 1B).

We first compared the labeling density between a 1:1,000 and 1:5,000 dilution of the Cre-encoding AAV in adult mice (~6 weeks old, hereafter referred to as "$CKO^{adult\ inj}$") to determine the optimal dilution to sparsely infect L5 PyrNs. The 1:1,000 dilution resulted in a labeling density of 364 ± 22 cells/mm^2, while the 1:5,000 dilution had a labeling density of 54 ± 8 cells/mm^2 (Figure 1C). I chose 1:5,000 dilution for all subsequent experiments as its labeling density was adequate

for *in vivo* imaging of dendritic branches and spines. The 1:5,000 Cre-encoding AAV dilution produced a viral spread of 2.2 ± 0.22 mm along the anterior-posterior axis, with the densest labeling at approximately -0.7 mm from the bregma (Figure 1D). The medial-lateral viral spread was 1.29 ± 0.2 mm, indicating an effective targeting of S1 (Figure 1D).

3.2 Virus-induced FMRP KO in single neurons in adolescent and adult mice

We next verified the specificity and effectiveness of the FMRP KO strategy with immunohistochemistry in both $CKO^{adult\ inj}$ mice and mice injected at postnatal day 1-3 (P1-3; Figure 2A-D). Mice injected at P1-3 will be hereafter referred to as "$CKO^{neo\ inj}$". After three weeks of virus incubation, we found in $CKO^{adult\ inj}$ mice that a sparse subset of L5 PyrNs were GFP+ (Figure 2B and D). Among these cells, only 5.3 ± 1.2% were FMRP+ (Figure 2E). Similarly, $CKO^{neo\ inj}$ mice exhibited sparse GFP labelling of L5 PyrNs (Figure 2C and D), and only 7.3 ± 1.1% of such cells were FMRP+ (Figure 2E). In contrast, wild type mice that received the same virus injection in adulthood ("$WT^{adult\ inj}$") continued to express FMRP in infected cells, with 94.5 ± 1.5% of GFP+ cells being FMRP+ (Figure 2E). These data confirm the effectiveness and specificity of our knockout strategy.

3.3 Single-cell FMRP KO does not alter spine density in adult mice

To assess the effects of single-cell *Fmr1* KO on the structural dynamics of dendritic spines, we performed longitudinal *in vivo* two-photon imaging on adult mice

through a cranial window (Holtmaat, Bonhoeffer et al. 2009). We first compared the density of spines on apical dendritic tufts of L5 PyrNs in $WT^{adult\ inj}$, $CKO^{adult\ inj}$, and GKO mice receiving virus injection in adulthood ("$GKO^{adult\ inj}$") when the mice reached 10 weeks of age (Figure 3A). We found that in $GKO^{adult\ inj}$ mice, the spine density was 0.43 ± 0.02/μm, significantly higher than that in $WT^{adult\ inj}$ mice (0.35 ± 0.02/μm; one-way ANOVA, $F(2,12) = 6.111$, $p < 0.05$; *post hoc* Dunnett's multiple comparisons test $p < 0.05$; Figure 3B), which is consistent with reports in the literature (Galvez and Greenough 2005). We further analyzed the density of spines in different morphological categories (Figure 3C). Only thin spines exhibited significant density difference between $GKO^{adult\ inj}$ and $WT^{adult\ inj}$ mice (two-way repeated measures ANOVA, $F(6, 36) = 10.02$, $p < 0.0001$; *post hoc* Dunnett's multiple comparisons test $p < 0.01$); the rest showed no difference (*post hoc* Dunnett's multiple comparisons test $p = 0.4707$, 0.6510, and 0.9983 for stubby, mushroom, and others, respectively). Interestingly, spine density in $CKO^{adult\ inj}$ mice (0.37 ± 0.01/μm) was not significantly different from that in $WT^{adult\ inj}$ mice (*post hoc* Dunnett's multiple comparisons test $p = 0.8378$; Figure 2B). Nor was there significant density difference in spines belonging to any morphological category between $CKO^{adult\ inj}$ and $WT^{adult\ inj}$ mice (*post hoc* Dunnett's multiple comparisons test $p = 0.9518$, 0.0955, 0.9908, and 0.1754 for stubby, mushroom, thin, and others, respectively).

3.4 Viral injection does not affect spine density

To control for the possibility that virus infection *per se* affects spine density, we also measured spine density in *Thy1*-GFP-M mice (which are *Fmr1*+, hence denoted "WT^{M}") as well as in GKO × *Thy1*-GFP-M ("GKO^{M}") mice. These animals express cytoplasmic GFP in a sparse subset of cortical L5 PyrNs, thus obviating the need for viral labeling. We found no difference in spine density between $WT^{adult\ inj}$ mice and WT^{M} mice, or between $GKO^{adult\ inj}$ and GKO^{M} mice (Figure 4). These results demonstrate that the viral knockout strategy *per se* does not affect spine density.

3.5 Single-cell FMRP KO does not alter spine density in adolescent mice

We next examined the effects of single-cell *Fmr1* KO on the structural dynamics of dendritic spines in the developing adolescent (P30) mouse brain by performing longitudinal *in vivo* two-photon imaging on adolescent mice through the thin skull preparation (Xu et al., 2009). We compared the spine density of adolescent WT^{M}, GKO^{M}, and $CKO^{neo\ inj}$ mice (Figure 5A). We found no significant difference among these three groups: the spine density was 0.43 ± 0.02/μm in WT^{M}, 0.44 ± 0.01/μm in GKO^{M}, and 0.46 ± 0.01/μm in $CKO^{neo\ inj}$ mice (one-way ANOVA, $F(2,13) = 1.421$, $p = 0.2766$; Figure 5B). This agrees with previous findings (Nimchinsky, Oberlander et al. 2001;Galvez and Greenough 2005;Pan, Aldridge et al. 2010;Hodges, Yu et al. 2017;Bland, Aharon et al. 2021). Furthermore, $CKO^{neo\ inj}$ mice showed no significant difference in the density of any spine type in comparison with WT^{M} mice (two-way repeated measures ANOVA, $F(3,27) = 0.4985$, $p = 0.6864$;

Figure 5C), similar to the previous report on adolescent GKO mice (Hodges, Yu et al. 2017).

3.6 Neither global nor single-cell FMRP KO affects the structural dynamics of dendritic spines in adult mice

We then examined the structural dynamics of spines in $WT^{adult\ inj}$, $GKO^{adult\ inj}$, and $CKO^{adult\ inj}$ mice starting at about 2 months of age, over 4-day and 16-day intervals (Figure 6). We found no significant difference in the rate of spine formation and elimination over 4 days: the spine formation rate was 4.4 ± 0.3% in $WT^{adult\ inj}$, 4.1 ± 0.3% in $GKO^{adult\ inj}$, and 3.8 ± 0.3% in $CKO^{adult\ inj}$ (one-way ANOVA, $F(2,12) = 1.017$, $p = 0.3907$; Figure 7A), and the spine elimination rate was 5.8 ± 0.4% in $WT^{adult\ inj}$, 5.9 ± 0.2% in $GKO^{adult\ inj}$, and 5.2 ± 0.3% in $CKO^{adult\ inj}$ (one-way ANOVA, $F(2,12) = 1.122$, $p = 0.3574$; Figure 7B). Likewise, there was no significant difference in spine dynamics over 16 days. The spine formation rate was 5.9 ± 0.4%, 6.0 ± 0.8%, and 5.5 ± 0.9% in $WT^{adult\ inj}$, $GKO^{adult\ inj}$, and $CKO^{adult\ inj}$, respectively (one-way ANOVA, $F(2,12) = 0.1352$, $p = 0.8748$; Figure 7C), and the corresponding spine elimination rate was 8.6 ± 0.5% in $WT^{adult\ inj}$, 9.6 ± 0.3% in $GKO^{adult\ inj}$, and 8.7 ± 0.9% in $CKO^{adult\ inj}$ (one-way ANOVA, $F(2,12) = 0.7999$, $p = 0.4719$; Figure 7D). Following new spines formed by day 4 till day 16, we found no significant difference in their survival rate ($WT^{adult\ inj}$ 34.0 ± 10.7%, $GKO^{adult\ inj}$ 22.5 ± 6.7%, $CKO^{adult\ inj}$ 26.7 ± 8.5%; one-way ANOVA, $F(2,12) = 0.4419$, $p = 0.6529$; Figure 7E). These

results suggest that deleting FMRP from single neurons in adulthood does not affect its spine dynamics.

3.7 Viral injection does not affect structural dynamics of dendritic spines

Again, to control for potential confounding effects of virus infection, we measured spine dynamics in WT^{M} and GKO^{M} mice at comparable ages. Spine dynamics did not differ significantly between $WT^{adult\ inj}$ and WT^{M} mice, or between $GKO^{adult\ inj}$ and GKO^{M} mice (Figure 8). This confirms that the viral labeling strategy does not affect spine dynamics either and validates the use of WT^{M} and GKO^{M} mice as controls in adolescent studies.

3.8 Single-cell FMRP KO results in elevated dendritic spine formation in adolescent mice

As previous studies suggest that *Fmr1* KO affects spine dynamics most prominently in adolescence (Hodges, Yu et al. 2017), we examined 4-day and 16-day spine dynamics in $CKO^{neo\ inj}$, WT^{M}, and GKO^{M} mice starting at 1 month of age (Figure 9). We found that spine formation over 4 days was significantly elevated in $CKO^{neo\ inj}$ mice (7.4 ± 0.3%) and GKO^{M} mice (8.1 ± 0.5%) compared to WT^{M} mice (4.6 ± 0.3%; one-way ANOVA, $F(2,13) = 23.71$, $p < 0.001$; *post hoc* Dunnett's multiple comparisons test: $p < 0.001$ for $CKO^{neo\ inj}$ vs WT^{M} and for GKO^{M} vs WT^{M}; Figure 10A). However, spine elimination over 4 days was unaffected (WT^{M} 7.2 ± 0.4%, GKO^{M}: 6.5 ± 0.4%, $CKO^{neo\ inj}$: 6.7 ± 0.3%; one-way ANOVA, $F(2,13)$ =

1.225, $p = 0.3255$; Figure 10B). A similar phenomenon emerged over the 16-day interval: $CKO^{neo\ inj}$ mice had a spine formation rate of 13.5 ± 1.1%, which was comparable to that in GKO^{M} mice (13.7 ± 0.3%) but differed significantly from that in WT^{M} mice (9.2 ± 0.5%; one-way ANOVA, $F(2,12) = 12.05$, $p < 0.01$; *post hoc* Dunnett's multiple comparisons test: $p < 0.01$ for both $CKO^{neo\ inj}$ vs WT^{M} and GKO^{M} vs WT^{M}; Figure 10C). The 16-day spine elimination did not significantly differ among the three groups, with rates of 13.3 ± 0.4% (WT^{M}), 13.8 ± 0.4% (GKO^{M}), and 13.9 ± 0.9% ($CKO^{neo\ inj}$), respectively (one-way ANOVA, $F(2,12) = 0.3124$, $p = 0.7374$; Figure 10D).

3.9 Single-cell FMRP KO in adolescence results in elevated density of thin spines in adulthood, but not overall increased spine density

We further followed $CKO^{neo\ inj}$ mice into adulthood and re-examined their spine density and morphology. To our surprise, spine density on the FMRP-null neurons was comparable to that in $WT^{adult\ inj}$ mice (unpaired *t*-test, $t(8) = 1.116$, $p = 0.2966$; Figure 11A). Morphological analysis, however, revealed an elevated density of thin spines on FMRP-null neurons (two-way repeated measures ANOVA, $F(3,24) = 22.56$, $p < 0.0001$; *post hoc* Šidák multiple comparisons test, $p < 0.01$; Figure 11B). The normalization of total spine density was due to decreased density of all other types of spines. Together with findings in adult animals, these results suggest that FMRP regulates the structural dynamics of spines cell-autonomously in adolescence,

but the development of spine defects into adulthood also involves non-cell-autonomous factors.

CHAPTER 4: DISCUSSION

4.1 Isolation of FMRP function from network effects

The abundance of dendritic spines with an immature morphology in the adult brain is an anatomical hallmark of FXS in humans and in mouse models. Traditionally, it is conjectured that this phenotype results from defective spine pruning during development (Greenough, Klintsova et al. 2001;Churchill, Grossman et al. 2002;Bagni and Greenough 2005;Bardoni, Davidovic et al. 2006). More recent *in vivo* imaging studies, however, reveal elevated spine formation in adolescence (Pan, Aldridge et al. 2010;Padmashri, Reiner et al. 2013;Nagaoka, Takehara et al. 2016;Hodges, Yu et al. 2017), and some of them in addition suggest that spine elimination during this developmental stage is elevated as well. The cellular underpinning of such altered structural dynamics is likely complex. It may involve abnormal neural activity patterns operating through activity-dependent mechanisms to prevent the maturation of new spines and the competitive removal of weak and immature spines. It may also implicate altered intrinsic excitability of neurons due to ion channel dysregulation, excitation/inhibition imbalance induced by dysfunctional local inhibitory circuits, and altered homeostatic plasticity (Gibson, Bartley et al. 2008;Soden and Chen 2010;Goel, Cantu et al. 2018;Liu, Kumar et al. 2021). Moreover, astrocytes may contribute to the spine pathology, as astrocyte-specific KO of *Fmr1* suffices to elevate spine formation (Hodges, Yu et al. 2017). Other studies in addition suggests altered inflammatory response of microglia (Parrott, Oster et al. 2021) and reduced microglia-mediated synaptic pruning (Jawaid, Kidd et al. 2018) in

Fmr1 global KO mice. Such a plethora of participants makes it difficult to disentangle the contribution of cell-autonomous dysregulation from that of external factors, if *Fmr1* is knocked out globally. In fact, even studies that leverage the random X-linked inactivation of *Fmr1* in heterozygous females to generate mosaicism (approximately half of the neurons are FMRP-null and the other half FMRP+) still suffer from the caveat that network effects cannot be ruled out (Bland, Aharon et al. 2021).

In this study, we circumvented this problem by a virus-based strategy to induce *Fmr1* KO only in a very small subset of cortical PyrNs. Thus, the perturbation to the activity pattern in the neuronal network is negligible. Furthermore, as each PyrN receives thousands of inputs (Iascone, Li et al. 2020), the vast majority of them are from neurons that express FMRP normally. We observed that in adolescent $CKO^{neo\ inj}$ mice, FMRP-null neurons exhibited the same spine dynamics as in *Fmr1* global KO mice, indicating that FMRP regulates spine dynamics cell-autonomously at this developmental stage. This result is consistent with a recent electrophysiological study (Zhang, Gibson et al. 2021) showing that virus-based cell-autonomous deletion of FMRP from L2/3 or L5 neurons weakens callosal excitatory synapses. It is also consistent with the earlier study (Pfeiffer and Huber 2007) showing that acute, postsynaptic expression of FMRP in *Fmr1* KO neurons *in vitro* reduces their synapse number. This suggests that in *Fmr1* global KO mice, which more realistically reflect the condition in FXS patients, the lack of FMRP in the neurons to which the spines belong is the determining factor of the pathology in spine density and dynamics. Interestingly, although neurons with neonatal FMRP deletion

exhibit abnormally high density of thin spines when the animal reaches adulthood, the total spine density remains at the WT level. In contrast, the elevated density of thin spines on neurons in adult GKO mice increases total spine density as well. This intriguing phenomenon calls for further investigations into the contribution of the neuronal network and other extrinsic factors. It is worth noting that the regulation of spine dynamics by FMRP does not imply that the effect is mediated completely intracellularly. It has been reported that genetic deletion of matrix metalloproteinase-9 (MMP-9), an FMRP target enzyme involved in the degradation of the extracellular matrix, can rescue spine morphological and behavioral deficits in *Fmr1* global KO mice (Sidhu, Dansie et al. 2014). Another work shows that injecting an MMP-9 inhibitor likewise rescues the baseline spine dynamics in such animals (Nagaoka, Takehara et al. 2016).

4.2 Diving deeper than apical dendrites in layer 1 of cortex

Most *in vivo* imaging studies of spine dynamics in FXS focus on the apical dendrites of L5 PyrNs, leveraging the sparse but very bright neuronal labeling conveniently offered by the *Thy1*-YFP-H or *Thy1*-GFP-M line (Pan, Aldridge et al. 2010;Padmashri, Reiner et al. 2013;Nagaoka, Takehara et al. 2016;Hodges, Yu et al. 2017). However, there is evidence that FMRP regulates spine morphology differentially in different compartments of the dendritic arbor. For example, a histological study (Bland, Aharon et al. 2021) shows that *Fmr1* KO or inactivation affects the density of spines on basal dendrites of L5 PyrNs minimally. It will be

interesting to examine whether the dynamics of such spines are altered by the loss of FMRP; such experiments have become possible with recent advances in imaging techniques such as three-photon microscopy and adaptive optics (Rodriguez and Ji 2018;Sinefeld, Xia et al. 2022).

4.3 Input-specific regulation of synapses by FMRP

The regulatory role of postsynaptic FMRP may also be input-specific. A recent immunofluorescent array tomography study of cortical tissues from adult *Fmr1* global KO mice (Simhal, Zuo et al. 2019) revealed an increase of small synapses that expressed vesicular glutamate transport 1 (VGluT1+) in L4 and a decrease of large VGluT1+ synapses in L1 and L4; moreover, VGluT2+ synapse density consistently decreased in L1 and L2/3. As VGluT1+ and VGluT2+ excitatory synapses are generally considered to be corticocortical and thalamocortical, respectively, this work suggests an input-specific defect associated with *Fmr1* KO. More interestingly, it was recently found (Zhang, Gibson et al. 2021) that, while barrel cortex L2/3 neurons with cell-autonomous *Fmr1* KO had weaker long-range callosal synaptic connections, their excitatory postsynaptic currents (EPSCs) evoked by local inputs (L4 of home or adjacent barrels, L5A or L2/3 neurons) were unaffected. Similarly, L5 PyrNs with postsynaptic *Fmr1* KO had weakened callosal inputs around their somata and apical dendrites. These findings are intriguing, as only a very small percentage of the neurons were FMRP-null, and hence their presynaptic partners should be predominantly normal no matter where they resided. The mechanisms through which

postsynaptic FMRP differentially regulate the maturation and strength of synapses from different input sources remain to be elucidated.

FIGURES

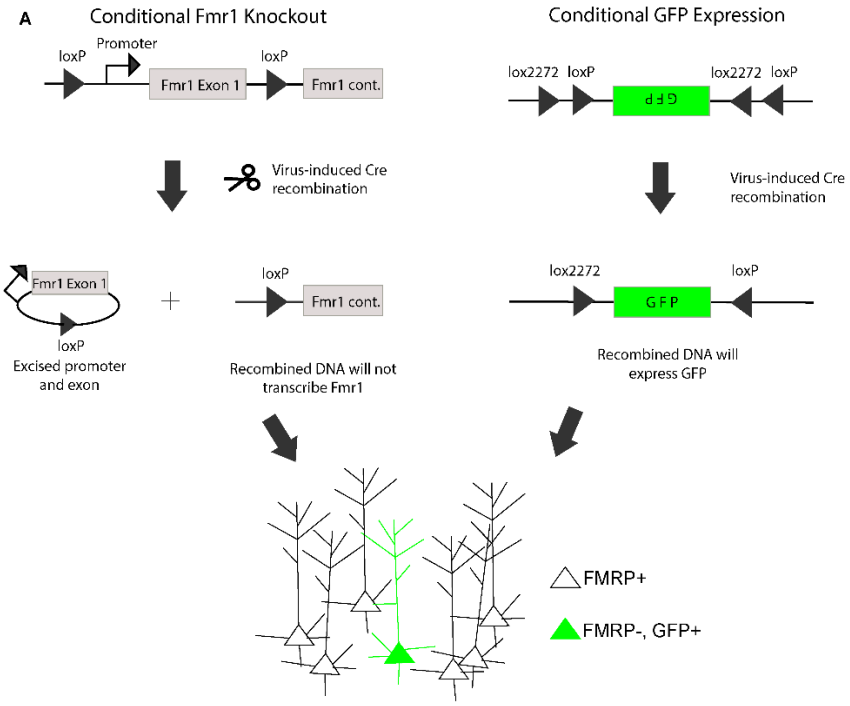
A
Conditional Fmr1 Knockout
loxP
Promoter
loxP
Fmr1 Exon 1
Fmr1 cont.
Virus-induced Cre recombination
Fmr1 Exon 1
loxP
Excised promoter and exon
loxP
Fmr1 cont.
Recombined DNA will not transcribe Fmr1
Conditional GFP Expression
lox2272 loxP
GFP
lox2272 loxP
Virus-induced Cre recombination
lox2272
loxP
GFP
Recombined DNA will express GFP
FMRP+
FMRP-, GFP+

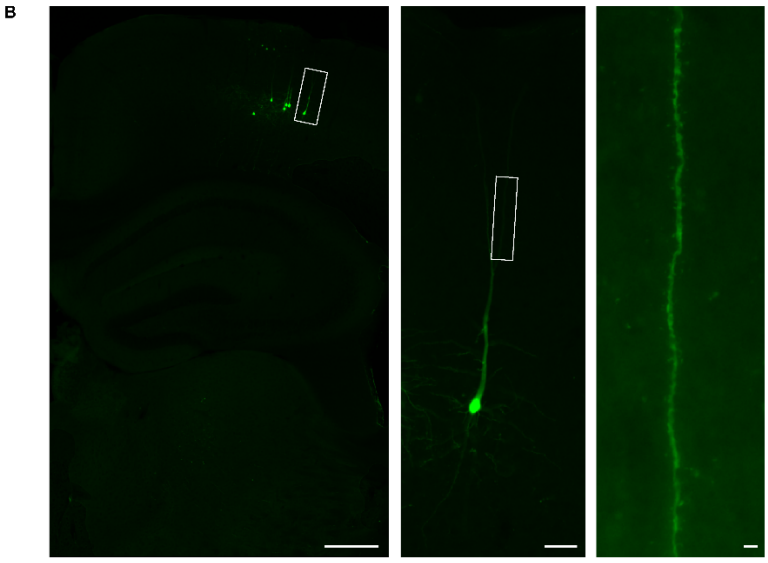
B

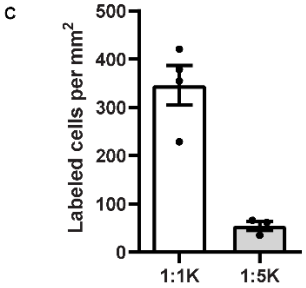
C
Labeled cells per mm2
500
400
300
200
100
0
1:1K
1:5K

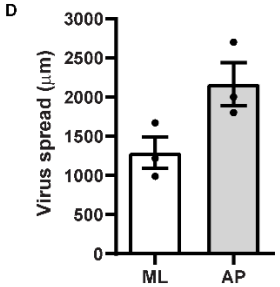
D
Virus spread (μm)
3000
2500
2000
1500
1000
500
0
ML
AP

Figure 1. Cre-lox recombination strategy sparsely labels L5 cortical pyramidal neurons for dendritic spine imaging.
A. Schematic of sparse Fmr1 conditional knockout strategy using a viral mixture of Cre and GFP-dependent Cre viruses in *Fmr1*$^{fl/y}$ mice. **B.** Example of labelling of apical dendrites and dendritic spines in an infected cell. Middle panel: labelled neuron in the white box of the left panel. Right panel: dendritic segment in the white box of the middle panel. Scale bars: 500 μm (left), 50 μm (middle), 10 μm (right). **C.** Labeling densities of different dilutions of Cre virus. Densities were calculated from the most densely labeled sections. **D.** Medial-lateral (ML) and anterior-posterior (AP) virus spread based on the locations of GFP+ soma. Data are presented as mean ± SEM.

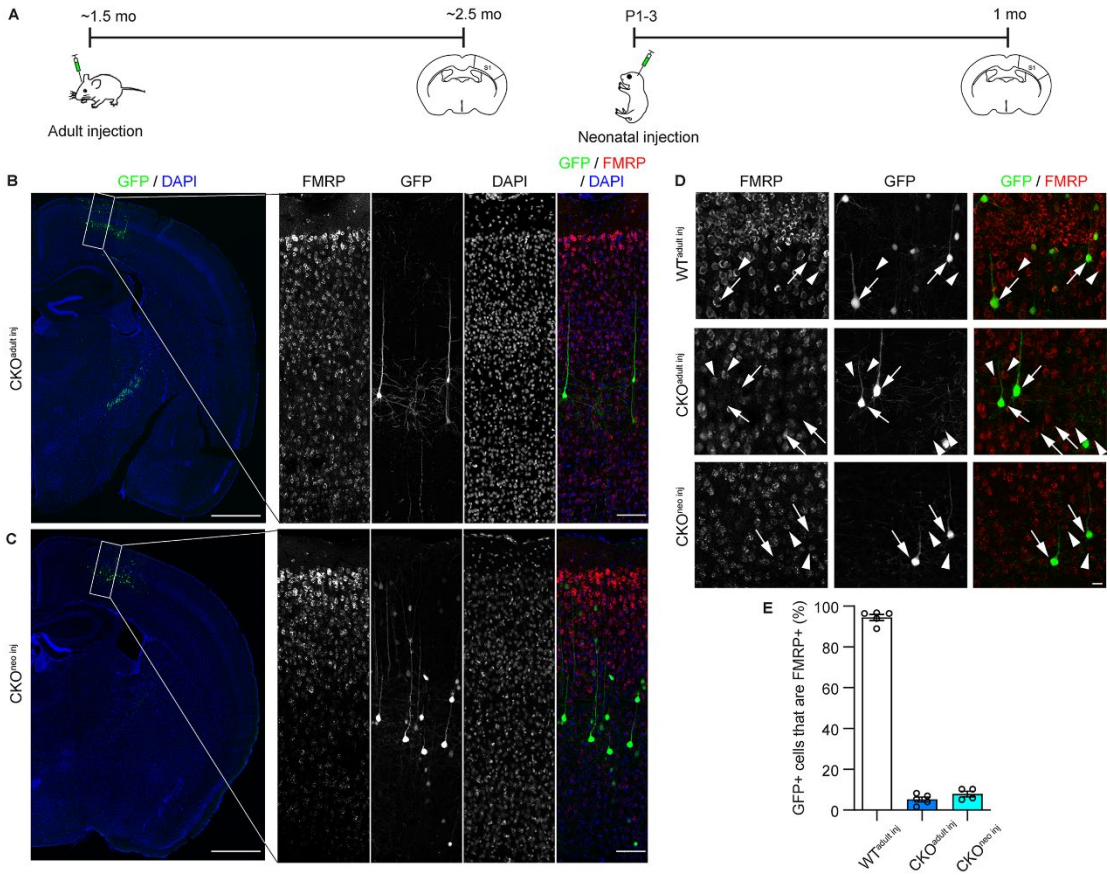

Figure 2. Virus-mediated cre-lox recombination successfully eliminates FMRP from individual infected cells.

A. Timeline of virus injection and histology. **B.** Left: example of Cre-dependent GFP expression and *Fmr1* KO in a sparse subset of S1 L5 PyrNs of a *Fmr1* CKO$^{\text{adult inj}}$ mouse. Scale bar: 500 µm. Right: Enlarged view of the rectangular region in the left panel showing FMRP and GFP expression. Scale bar: 100 µm. **C.** Examples of *Fmr1* KO in a CKO$^{\text{neo inj}}$ mouse, with the same magnification and arrangement as in (**B**). **D.** FMRP and GFP expression in WT$^{\text{adult inj}}$ (top), CKO$^{\text{adult inj}}$ (middle), and CKO$^{\text{neo inj}}$ (bottom) mice imaged with confocal microscopy. Arrows: GFP+ cells; arrowheads: GFP-/FMRP+ cells. Scale bar: 20 µm. **E.** Percentages of cells co-expressing GFP and FMRP in WT$^{\text{adult inj}}$, CKO$^{\text{adult inj}}$, and CKO$^{\text{neo inj}}$ mice. WT$^{\text{adult inj}}$ $n = 5$ mice (335 cells); CKO$^{\text{adult inj}}$ $n = 5$ mice (397 cells); CKO$^{\text{neo inj}}$ $n = 4$ mice (404 cells).

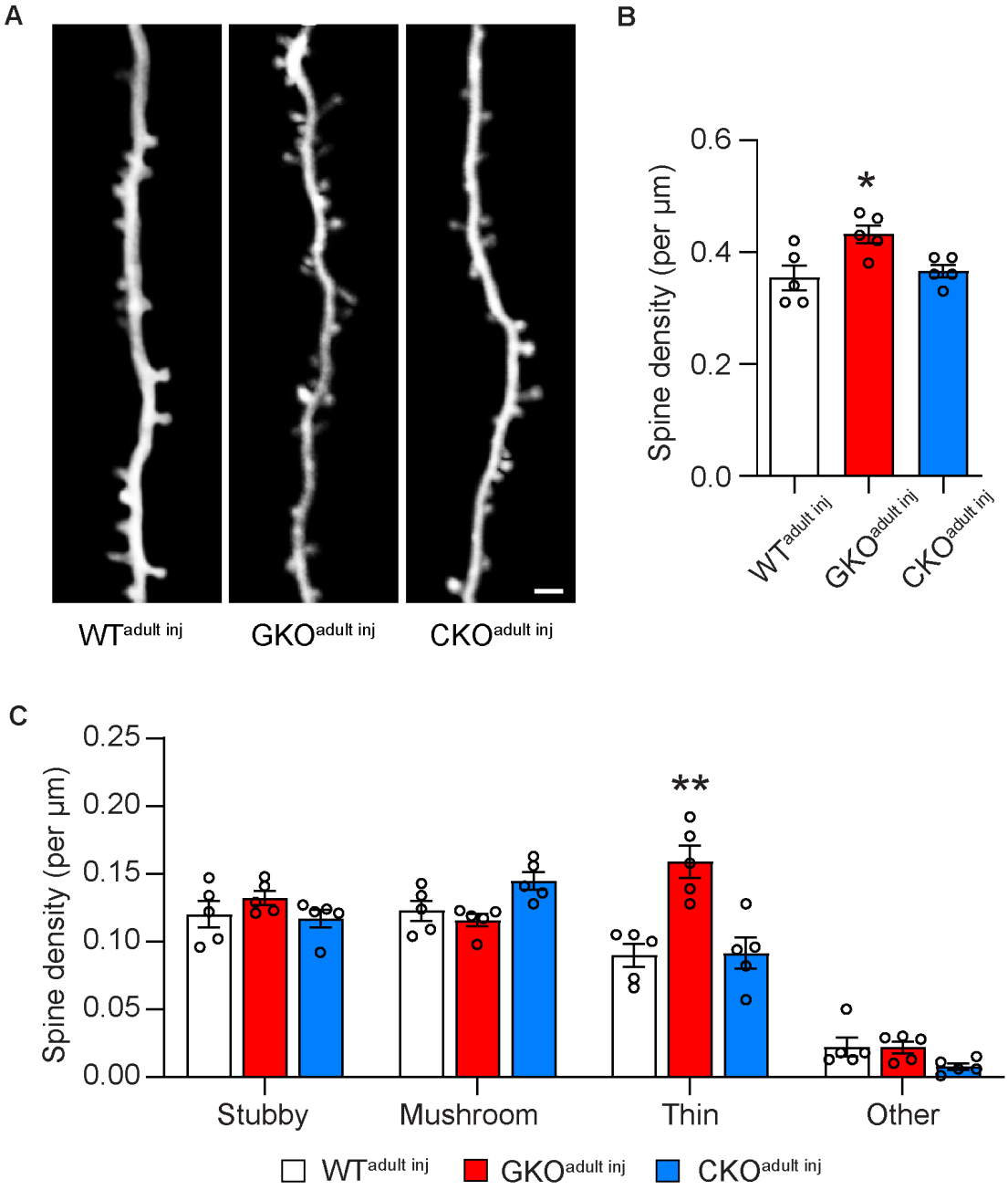

Figure 3. Cell-autonomous *Fmr1* knockout (KO) in adulthood does not alter spine density.

A. Examples of dendritic spines imaged *in vivo* in adult mice. **B.** Total spine density in $WT^{adult\ inj}$, $GKO^{adult\ inj}$, and $CKO^{adult\ inj}$ mice. n = 5 per group. **C.** Density of different types of spines in $WT^{adult\ inj}$, $GKO^{adult\ inj}$, and $CKO^{adult\ inj}$ mice. n = 5 per group. Scale bar = 2 µm. Hereinafter $*p < 0.05$, $**p < 0.01$, $***p < 0.001$; *post hoc* comparisons with the control group.

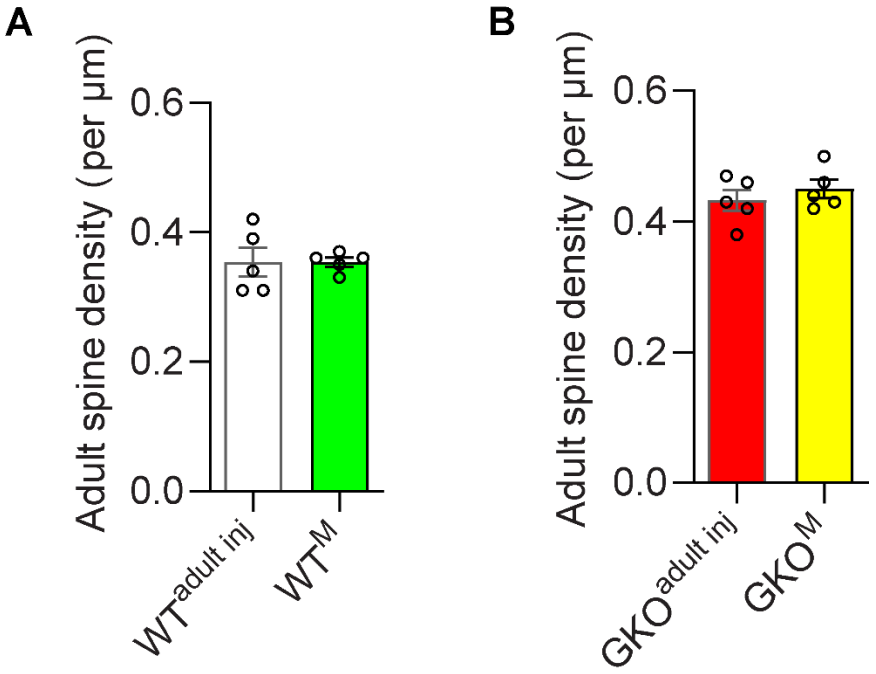

Figure 4. Virus injection *per se* does not affect spine density.
A. Spine density does not differ significantly between $WT^{adult\ inj}$ (0.35 ± 0.02 per µm) and WT^{M} (0.35 ± 0.01 per µm) mice. Unpaired *t*-test, $t(8) = 0.000$, $p > 0.999$. **B.** Spine density does not differ significantly $GKO^{adult\ inj}$ (0.43 ± 0.02 per µm) and GKO^{M} (0.45 ± 0.01 per µm) mice. Unpaired *t*-test, $t(8) = 0.8448$, $p = 0.4228$. $n = 5$ mice per group.

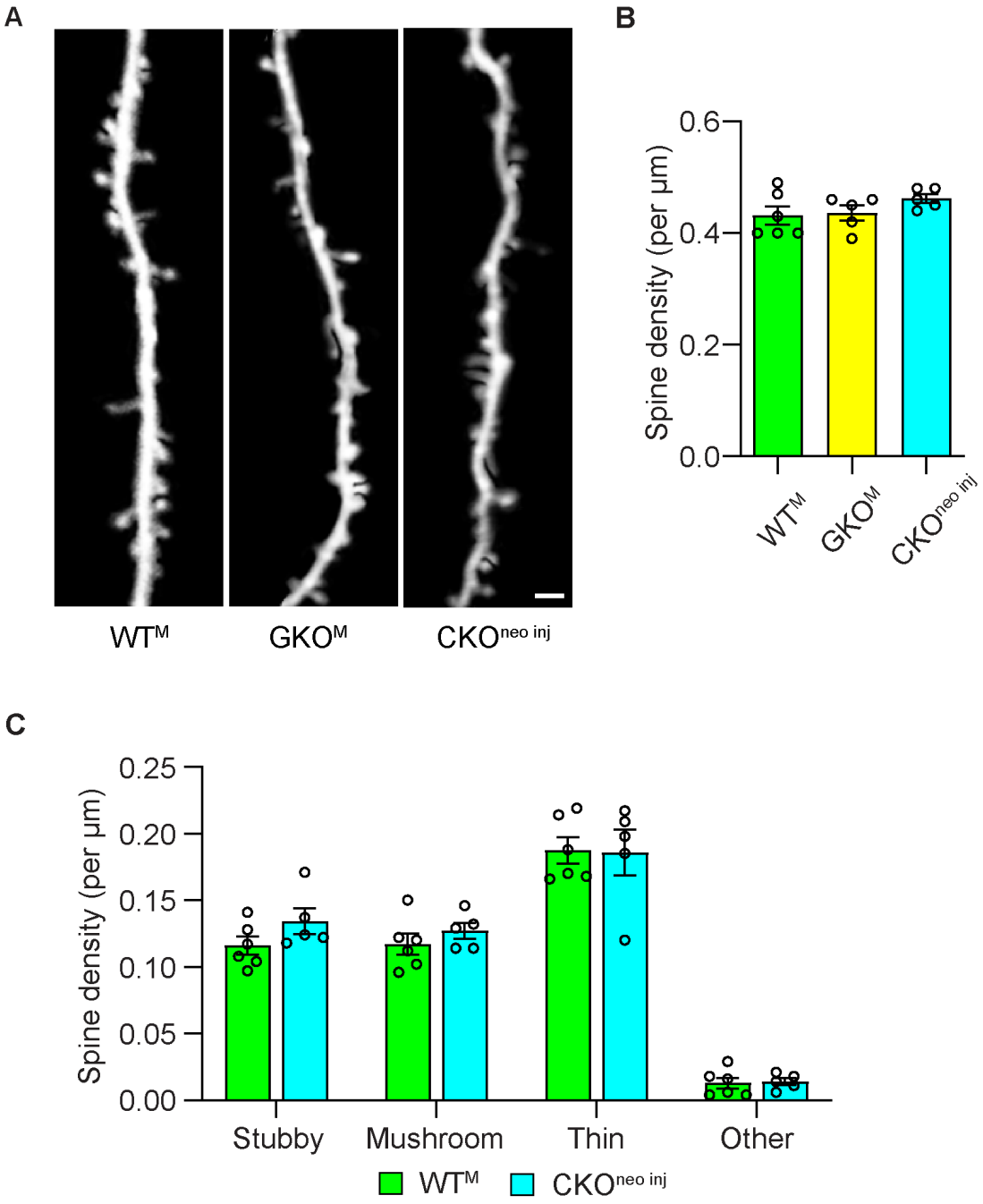

Figure 5. Cell-autonomous *Fmr1* knockout (KO) in adolescence does not alter spine density.

A. Examples of dendritic spines imaged *in vivo* in adolescent mice. **B.** Total spine density in adolescent mice. $n = 6$ for WT^{M}, 5 for GKO^{M} and $CKO^{neo\ inj}$ mice. **C.** Density of different types of spines in adolescent mice. $n = 6$ for WT^{M} and 5 for $CKO^{neo\ inj}$ mice. Scale bar = 2 µm.

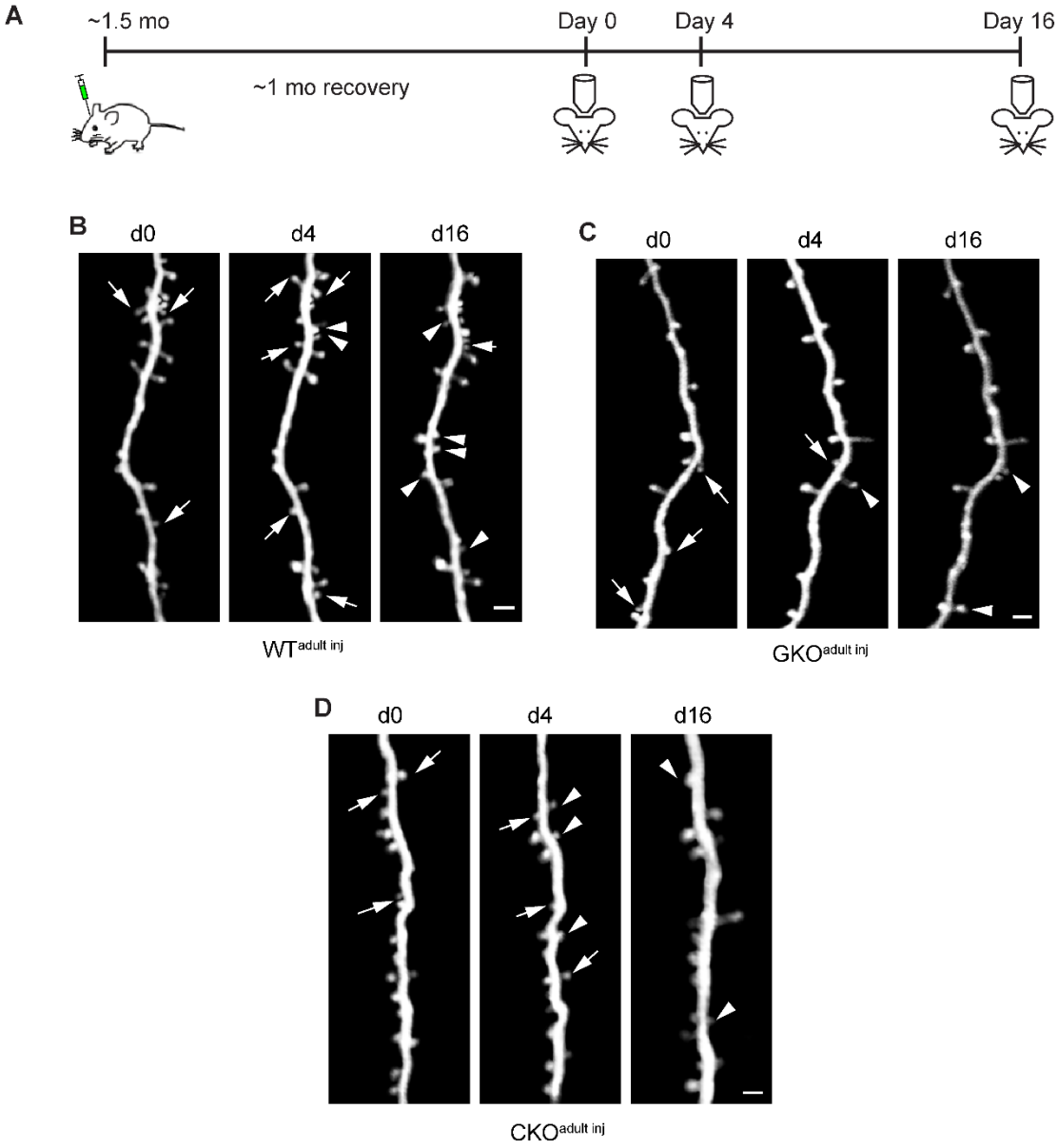

Figure 6. *In vivo* two photon imaging of cell-autonomous *Fmr1* KO in adulthood. **A.** Timeline of virus injection and *in vivo* two-photon imaging. **B-D.** Examples of spine formation and elimination in $WT^{adult\ inj}$ (**B**), $GKO^{adult\ inj}$ (**C**), and $CKO^{adult\ inj}$ (**D**) mice. Arrows: eliminated spines; arrowheads: formed spines. Scale bar = 2 μm.

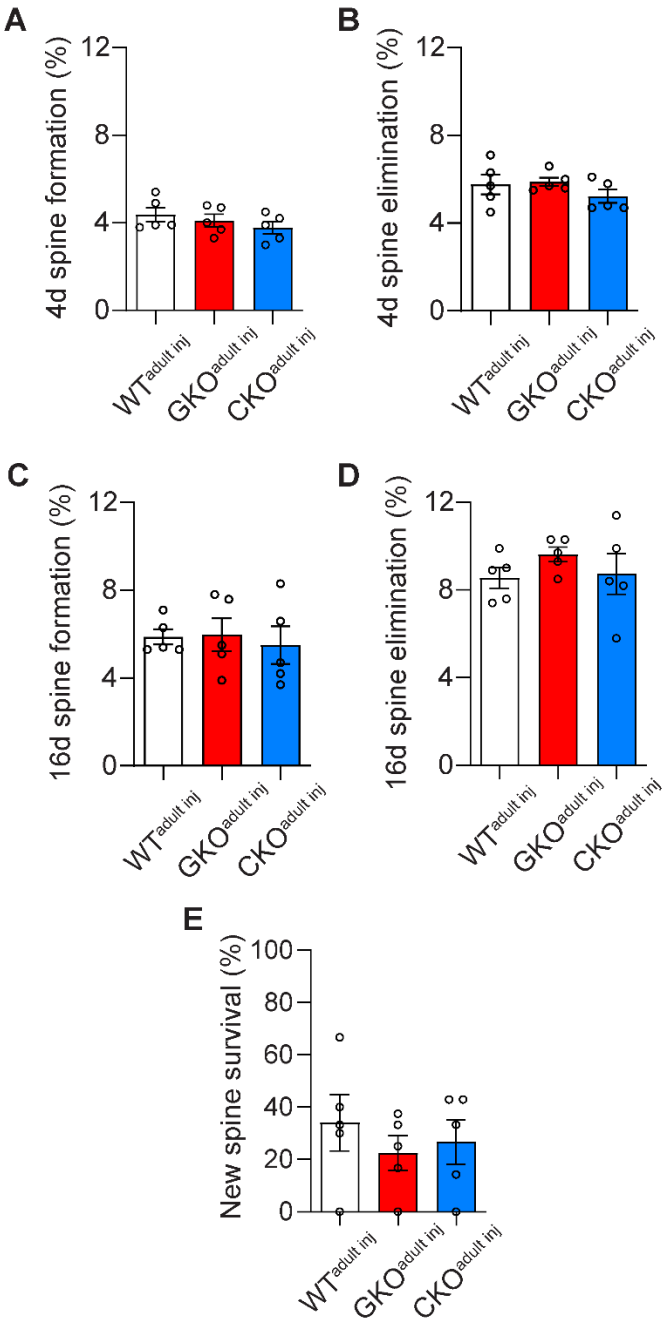

Figure 7. Cell-autonomous *Fmr1* KO in adulthood does not affect spine formation or elimination.

A-B. Spine formation (**A**) and elimination (**B**) rates over 4 days in WT$^{adult\ inj}$, GKO$^{adult\ inj}$, and CKO$^{adult\ inj}$ mice. **C-D.** Spine formation (**C**) and elimination (**D**) rates over 16 days in WT$^{adult\ inj}$, GKO$^{adult\ inj}$, and CKO$^{adult\ inj}$ mice. **E.** Percentage of new spines formed by day 4 that survived till day 16. n = 5 mice per group.

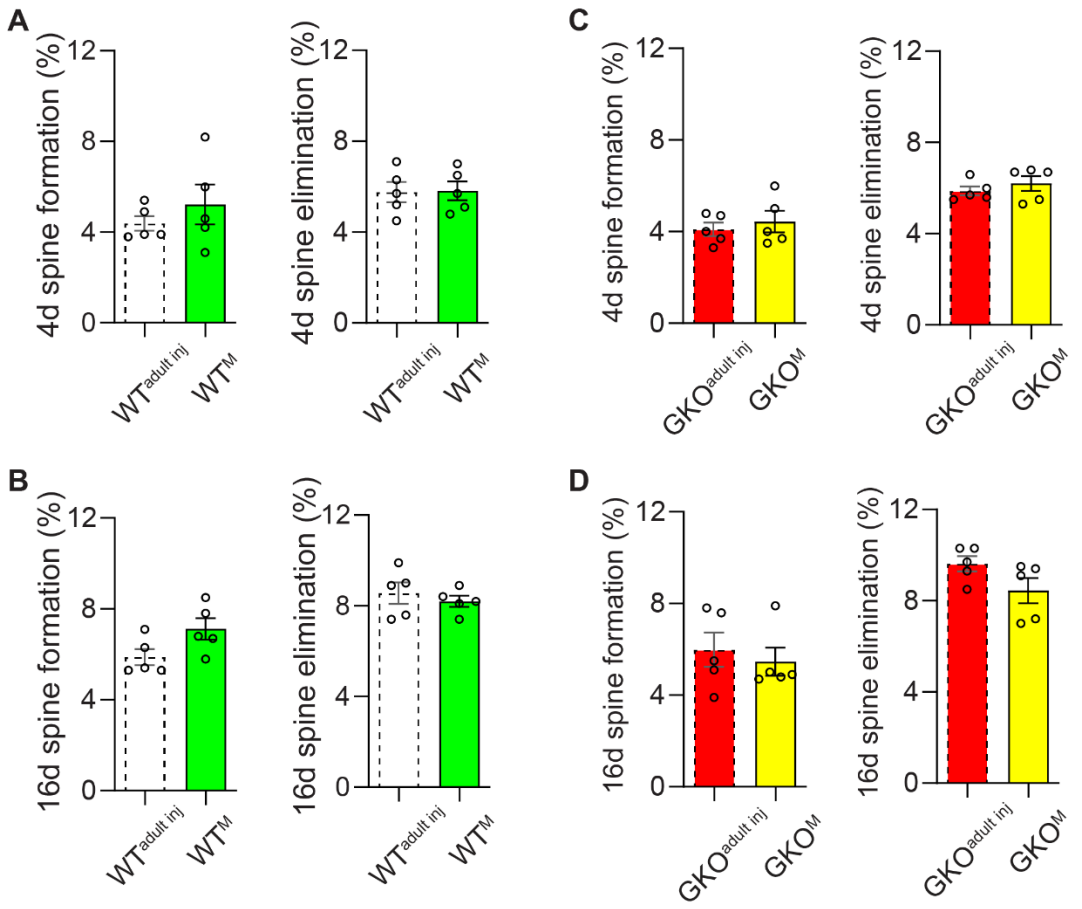

Figure 8. Virus injection *per se* does not affect spine dynamics.
A. Spine dynamics over 4 days do not differ between $WT^{adult\ inj}$ and WT^{M} mice. Formation: 4.4 ± 0.3% ($WT^{adult\ inj}$) vs 5.2 ± 0.9% (WT^{M}), unpaired *t*-test, $t(8) = 0.8976$, $p = 0.3956$. Elimination: 5.8 ± 0.4% ($WT^{adult\ inj}$) vs 5.8 ± 0.4% (WT^{M}), unpaired *t*-test, $t(8) = 0.0985$, $p = 0.9240$. **B.** Spine dynamics over 16 days do not differ between $WT^{adult\ inj}$ and WT^{M} mice. Formation: 5.9 ± 0.4% ($WT^{adult\ inj}$) vs 7.1 ± 0.5% (WT^{M}), unpaired *t*-test, $t(8) = 2.103$, $p = 0.0687$. Elimination: 8.6 ± 0.5% ($WT^{adult\ inj}$) vs 8.2 ± 0.2% (WT^{M}), unpaired *t*-test, $t(8) = 0.6833$, $p = 0.5137$. **C.** Spine dynamics over 4 days do not differ between $GKO^{adult\ inj}$ and GKO^{M} mice. Formation: 4.1 ± 0.3% ($GKO^{adult\ inj}$) vs 4.4 ± 0.5% (GKO^{M}), unpaired *t*-test, $t(8) = 0.6191$, $p = 0.5531$. Elimination: 5.9 ± 0.2% ($GKO^{adult\ inj}$) vs 6.2 ± 0.3% (GKO^{M}), unpaired *t*-test, $t(8) = 0.8335$, $p = 0.4287$. **D.** Spine dynamics over 16 days do not differ between $GKO^{adult\ inj}$ and GKO^{M} mice. Formation: 6.0 ± 0.8% ($GKO^{adult\ inj}$) vs 5.5 ± 0.6% (GKO^{M}), Mann-Whitney test, $U = 9$, $p = 0.5476$. Elimination: 9.6 ± 0.3% ($GKO^{adult\ inj}$) vs 8.4 ± 0.6% (GKO^{M}), unpaired *t*-test, $t(8) = 1.823$, $p = 0.1058$. $n = 5$ mice per group.

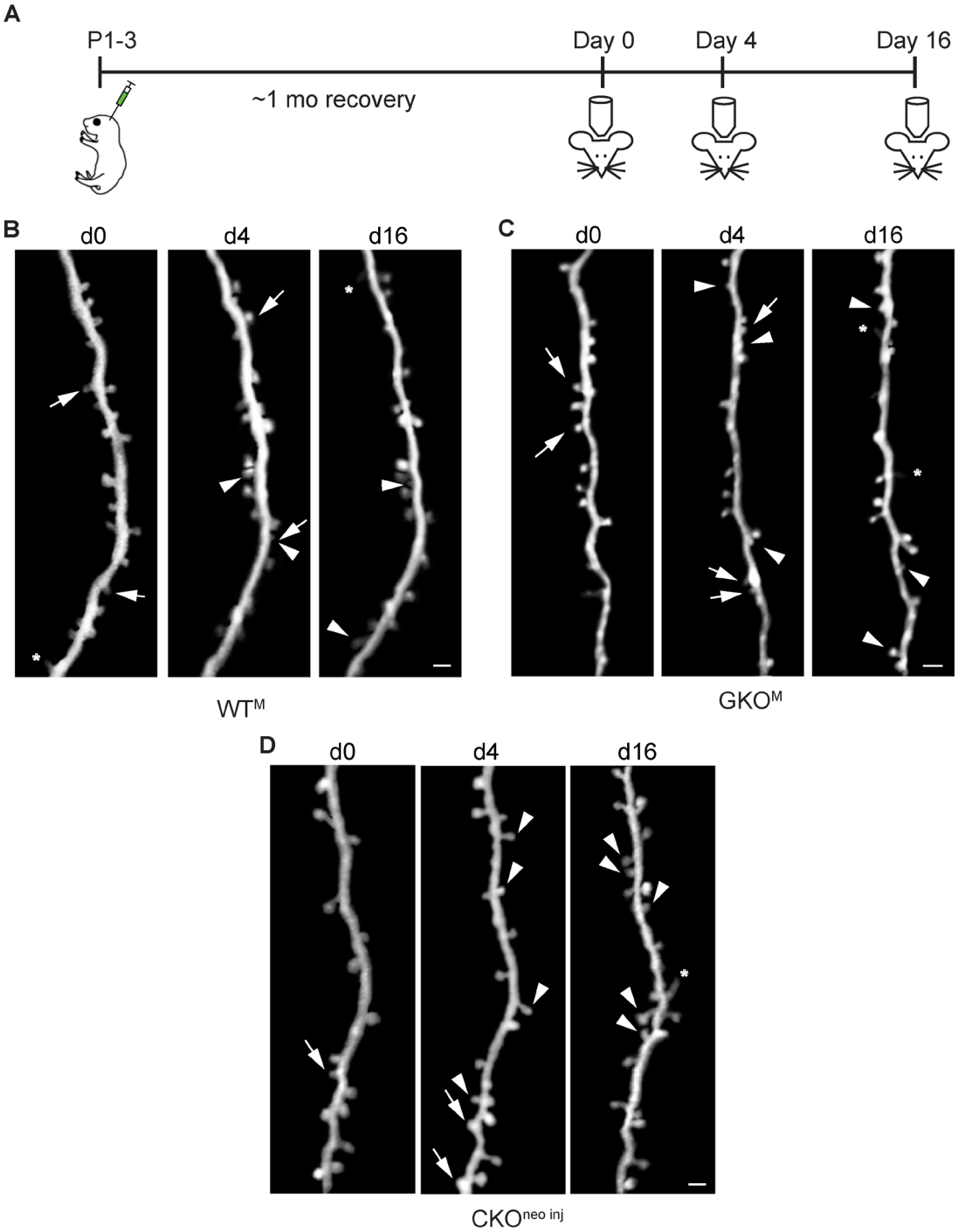

Figure 9. *In vivo* two photon imaging of cell-autonomous *Fmr1* KO in adolescence.

A. Timeline of virus injection and *in vivo* two-photon imaging. **B-D.** Examples of spine formation and elimination in adolescent WT^{M} (**B**), GKO^{M} (**C**), and $CKO^{neo\ inj}$ (**D**) mice. Arrows: eliminated spines; arrowheads: formed spines; asterisks: filopodia. Scale bar = 2 μm.

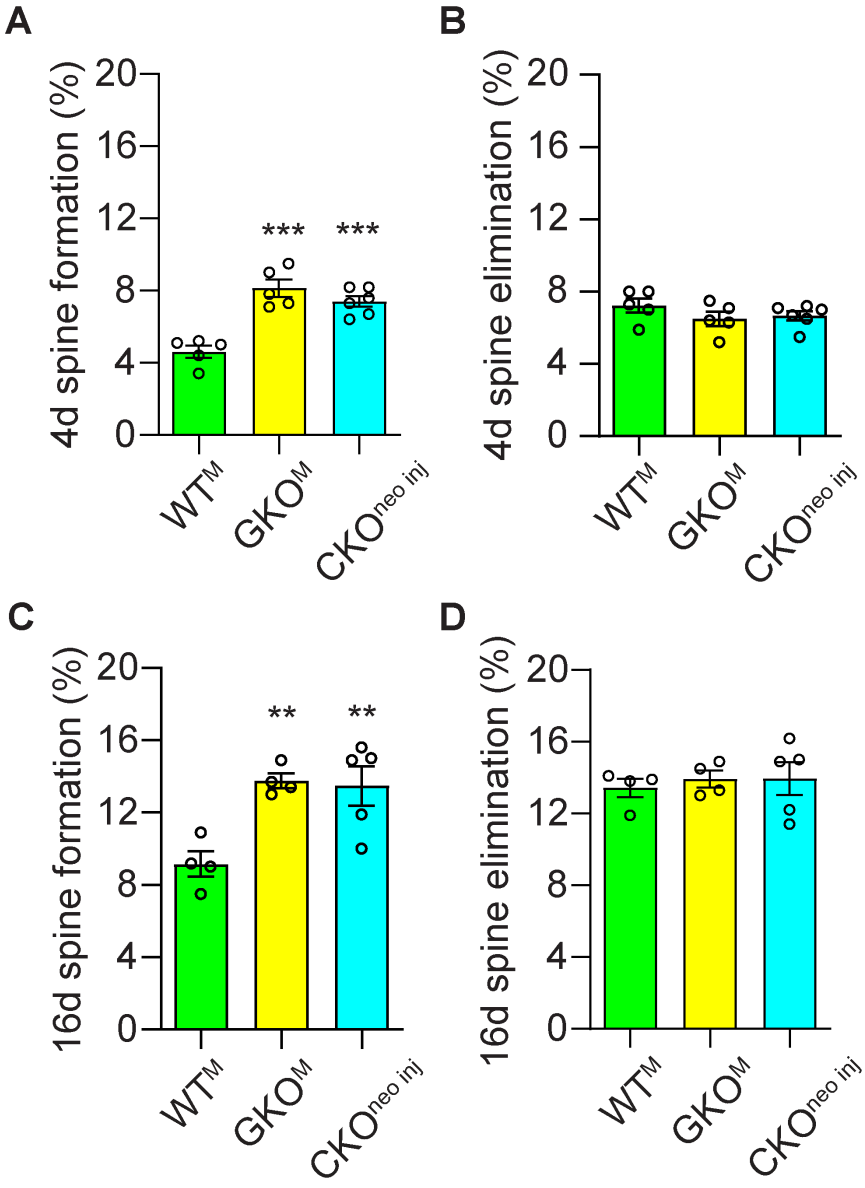

Figure 10. Cell-autonomous *Fmr1* KO in adolescence selectively affects spine formation but not elimination

A-B. Spine formation (**A**) and elimination (**B**) rates over 4 days in WT^{M}, GKO^{M}, and $CKO^{neo\ inj}$ mice. n = 5 mice for WT^{M} and GKO^{M}, and 6 mice for $CKO^{neo\ inj}$. **C-D.** Spine formation (**C**) and elimination (**D**) rates over 16 days in WT^{M}, GKO^{M}, and $CKO^{neo\ inj}$ mice. n = 5 mice per group.

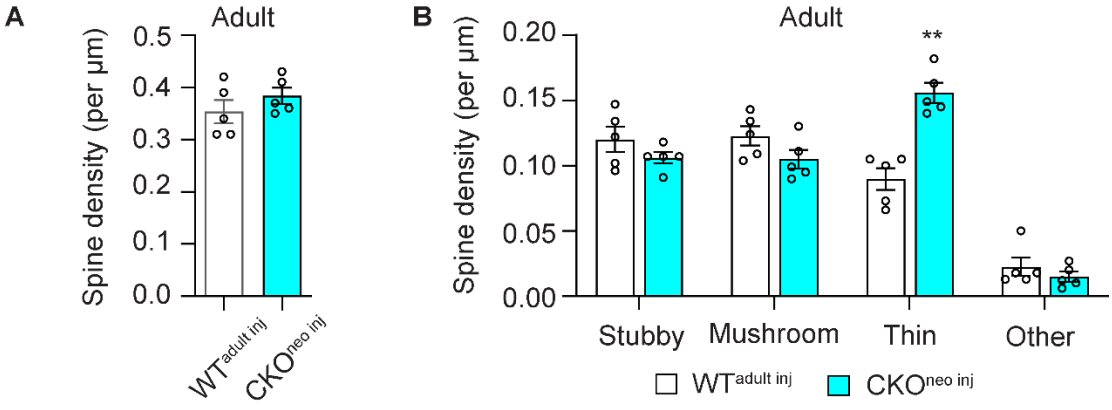

Figure 11. Single-cell FMRP knockout in adolescence results in elevated density of thin spines in adulthood, but not overall increased spine density.
A. Total spine density in $WT^{adult\ inj}$ and $CKO^{neo\ inj}$ mice at adulthood. $n = 5$ mice per group. **B.** Density of different types of spines in $WT^{adult\ inj}$ and $CKO^{neo\ inj}$ mice at adulthood. $n = 5$ mice per group.

REFERENCES

Antar, L. N., R. Afroz, J. B. Dictenberg, R. C. Carroll and G. J. Bassell (2004). "Metabotropic glutamate receptor activation regulates fragile x mental retardation protein and FMR1 mRNA localization differentially in dendrites and at synapses." J Neurosci **24**(11): 2648-2655.

Arbab, T., F. P. Battaglia, C. M. A. Pennartz and C. A. Bosman (2018). "Abnormal hippocampal theta and gamma hypersynchrony produces network and spike timing disturbances in the Fmr1-KO mouse model of Fragile X syndrome." Neurobiol Dis **114**: 65-73.

Arroyo, E. D., D. Fiole, S. S. Mantri, C. Huang and C. Portera-Cailliau (2019). "Dendritic Spines in Early Postnatal Fragile X Mice Are Insensitive to Novel Sensory Experience." J Neurosci **39**(3): 412-419.

Ashley, C. T., J. S. Sutcliffe, C. B. Kunst, H. A. Leiner, E. E. Eichler, D. L. Nelson and S. T. Warren (1993). "Human and murine FMR-1: alternative splicing and translational initiation downstream of the CGG-repeat." Nat Genet **4**(3): 244-251.

Bagni, C. and W. T. Greenough (2005). "From mRNP trafficking to spine dysmorphogenesis: the roots of fragile X syndrome." Nat Rev Neurosci **6**(5): 376-387.

Bardoni, B., L. Davidovic, M. Bensaid and E. W. Khandjian (2006). "The fragile X syndrome: exploring its molecular basis and seeking a treatment." Expert Rev Mol Med **8**(8): 1-16.

Bassell, G. J. and S. T. Warren (2008). "Fragile X syndrome: loss of local mRNA regulation alters synaptic development and function." Neuron **60**(2): 201-214.

Beckel-Mitchener, A. and W. T. Greenough (2004). "Correlates across the structural, functional, and molecular phenotypes of fragile X syndrome." Ment Retard Dev Disabil Res Rev **10**(1): 53-59.

Berry-Kravis, E. (2002). "Epilepsy in fragile X syndrome." Dev Med Child Neurol **44**(11): 724-728.

Bland, K. M., A. Aharon, E. L. Widener, M. I. Song, Z. O. Casey, Y. Zuo and G. S. Vidal (2021). "FMRP regulates the subcellular distribution of cortical dendritic spine density in a non-cell-autonomous manner." Neurobiol Dis **150**: 105253.

Bontekoe, C. J., E. de Graaff, I. M. Nieuwenhuizen, R. Willemsen and B. A. Oostra (1997). "FMR1 premutation allele (CGG)81 is stable in mice." Eur J Hum Genet **5**(5): 293-298.

Chen, C. C., J. Lu, R. Yang, J. B. Ding and Y. Zuo (2018). "Selective activation of parvalbumin interneurons prevents stress-induced synapse loss and perceptual defects." Mol Psychiatry **23**(7): 1614-1625.

Cheyne, J. E., N. Zabouri, D. Baddeley and C. Lohmann (2019). "Spontaneous Activity Patterns Are Altered in the Developing Visual Cortex of the Fmr1 Knockout Mouse." Front Neural Circuits **13**: 57.

Chmielewska, J. J., B. Kuzniewska, J. Milek, K. Urbanska and M. Dziembowska (2019). "Neuroligin 1, 2, and 3 Regulation at the Synapse: FMRP-Dependent Translation and Activity-Induced Proteolytic Cleavage." Mol Neurobiol **56**(4): 2741-2759.

Churchill, J. D., A. W. Grossman, S. A. Irwin, R. Galvez, A. Y. Klintsova, I. J. Weiler and W. T. Greenough (2002). "A converging-methods approach to fragile X syndrome." Dev Psychobiol **40**(3): 323-338.

Comery, T. A., J. B. Harris, P. J. Willems, B. A. Oostra, S. A. Irwin, I. J. Weiler and W. T. Greenough (1997). "Abnormal dendritic spines in fragile X knockout mice: maturation and pruning deficits." Proc Natl Acad Sci U S A **94**(10): 5401-5404.

Cruz-Martín, A., M. Crespo and C. Portera-Cailliau (2010). "Delayed stabilization of dendritic spines in fragile X mice." J Neurosci **30**(23): 7793-7803.

Darnell, J. C., S. J. Van Driesche, C. Zhang, K. Y. Hung, A. Mele, C. E. Fraser, E. F. Stone, C. Chen, J. J. Fak, S. W. Chi, D. D. Licatalosi, J. D. Richter and R. B. Darnell (2011). "FMRP stalls ribosomal translocation on mRNAs linked to synaptic function and autism." Cell **146**(2): 247-261.

Diering, G. H. and R. L. Huganir (2018). "The AMPA Receptor Code of Synaptic Plasticity." Neuron **100**(2): 314-329.

Entezam, A., R. Biacsi, B. Orrison, T. Saha, G. E. Hoffman, E. Grabczyk, R. L. Nussbaum and K. Usdin (2007). "Regional FMRP deficits and large repeat expansions into the full mutation range in a new Fragile X premutation mouse model." Gene **395**(1-2): 125-134.

Ferrari, F., V. Mercaldo, G. Piccoli, C. Sala, S. Cannata, T. Achsel and C. Bagni (2007). "The fragile X mental retardation protein-RNP granules show an mGluR-dependent localization in the post-synaptic spines." Mol Cell Neurosci **34**(3): 343-354.

Galvez, R. and W. T. Greenough (2005). "Sequence of abnormal dendritic spine development in primary somatosensory cortex of a mouse model of the fragile X mental retardation syndrome." Am J Med Genet A **135**(2): 155-160.

Giampetruzzi, A., J. H. Carson and E. Barbarese (2013). "FMRP and myelin protein expression in oligodendrocytes." Mol Cell Neurosci **56**: 333-341.

Gibson, J. R., A. F. Bartley, S. A. Hays and K. M. Huber (2008). "Imbalance of neocortical excitation and inhibition and altered UP states reflect network hyperexcitability in the mouse model of fragile X syndrome." J Neurophysiol **100**(5): 2615-2626.

Goel, A., D. A. Cantu, J. Guilfoyle, G. R. Chaudhari, A. Newadkar, B. Todisco, D. de Alba, N. Kourdougli, L. M. Schmitt, E. Pedapati, C. A. Erickson and C. Portera-Cailliau (2018). "Impaired perceptual learning in a mouse model of Fragile X syndrome is mediated by parvalbumin neuron dysfunction and is reversible." Nat Neurosci **21**(10): 1404-1411.

Gonzalez, D., M. Tomasek, S. Hays, V. Sridhar, S. Ammanuel, C. W. Chang, K. Pawlowski, K. M. Huber and J. R. Gibson (2019). "Audiogenic Seizures in the Fmr1 Knock-Out Mouse Are Induced by Fmr1 Deletion in Subcortical, VGlut2-Expressing Excitatory Neurons and Require Deletion in the Inferior Colliculus." J Neurosci **39**(49): 9852-9863.

Greenough, W. T., A. Y. Klintsova, S. A. Irwin, R. Galvez, K. E. Bates and I. J. Weiler (2001). "Synaptic regulation of protein synthesis and the fragile X protein." Proc Natl Acad Sci U S A **98**(13): 7101-7106.

Grossman, A. W., N. M. Elisseou, B. C. McKinney and W. T. Greenough (2006). "Hippocampal pyramidal cells in adult Fmr1 knockout mice exhibit an immature-appearing profile of dendritic spines." Brain Res **1084**(1): 158-164.

Hays, S. A., K. M. Huber and J. R. Gibson (2011). "Altered neocortical rhythmic activity states in Fmr1 KO mice are due to enhanced mGluR5 signaling and involve changes in excitatory circuitry." J Neurosci **31**(40): 14223-14234.

He, C. X., D. A. Cantu, S. S. Mantri, W. A. Zeiger, A. Goel and C. Portera-Cailliau (2017). "Tactile Defensiveness and Impaired Adaptation of Neuronal Activity in the Fmr1 Knock-Out Mouse Model of Autism." J Neurosci **37**(27): 6475-6487.

Hering, H. and M. Sheng (2001). "Dendritic spines: structure, dynamics and regulation." Nat Rev Neurosci **2**(12): 880-888.

Higashimori, H., C. S. Schin, M. S. Chiang, L. Morel, T. A. Shoneye, D. L. Nelson and Y. Yang (2016). "Selective Deletion of Astroglial FMRP Dysregulates Glutamate Transporter GLT1 and Contributes to Fragile X Syndrome Phenotypes In Vivo." J Neurosci **36**(27): 7079-7094.

Hinds, H. L., C. T. Ashley, J. S. Sutcliffe, D. L. Nelson, S. T. Warren, D. E. Housman and M. Schalling (1993). "Tissue specific expression of FMR-1 provides evidence for a functional role in fragile X syndrome." Nat Genet **3**(1): 36-43.

Hinton, V. J., W. T. Brown, K. Wisniewski and R. D. Rudelli (1991). "Analysis of neocortex in three males with the fragile X syndrome." Am J Med Genet **41**(3): 289-294.

Hodges, J. L., X. Yu, A. Gilmore, H. Bennett, M. Tjia, J. F. Perna, C. C. Chen, X. Li, J. Lu and Y. Zuo (2017). "Astrocytic Contributions to Synaptic and Learning Abnormalities in a Mouse Model of Fragile X Syndrome." Biol Psychiatry **82**(2): 139-149.

Holtmaat, A., T. Bonhoeffer, D. K. Chow, J. Chuckowree, V. De Paola, S. B. Hofer, M. Hubener, T. Keck, G. Knott, W. C. Lee, R. Mostany, T. D. Mrsic-Flogel, E. Nedivi, C. Portera-Cailliau, K. Svoboda, J. T. Trachtenberg and L. Wilbrecht (2009). "Long-term, high-resolution imaging in the mouse neocortex through a chronic cranial window." Nat Protoc **4**(8): 1128-1144.

Hunter, J., O. Rivero-Arias, A. Angelov, E. Kim, I. Fotheringham and J. Leal (2014). "Epidemiology of fragile X syndrome: a systematic review and meta-analysis." Am J Med Genet A **164A**(7): 1648-1658.

Iascone, D. M., Y. Li, U. Sumbul, M. Doron, H. Chen, V. Andreu, F. Goudy, H. Blockus, L. F. Abbott, I. Segev, H. Peng and F. Polleux (2020). "Whole-Neuron Synaptic Mapping Reveals Spatially Precise Excitatory/Inhibitory Balance Limiting Dendritic and Somatic Spiking." Neuron **106**(4): 566-578 e568.

Irwin, S. A., M. Idupulapati, M. E. Gilbert, J. B. Harris, A. B. Chakravarti, E. J. Rogers, R. A. Crisostomo, B. P. Larsen, A. Mehta, C. J. Alcantara, B. Patel, R. A. Swain, I. J. Weiler, B. A. Oostra and W. T. Greenough (2002). "Dendritic spine and dendritic field characteristics of layer V pyramidal neurons in the visual cortex of fragile-X knockout mice." Am J Med Genet **111**(2): 140-146.

Irwin, S. A., B. Patel, M. Idupulapati, J. B. Harris, R. A. Crisostomo, B. P. Larsen, F. Kooy, P. J. Willems, P. Cras, P. B. Kozlowski, R. A. Swain, I. J. Weiler and W. T. Greenough (2001). "Abnormal dendritic spine characteristics in the temporal and visual cortices of patients with fragile-X syndrome: a quantitative examination." Am J Med Genet **98**(2): 161-167.

Jawaid, S., G. J. Kidd, J. Wang, C. Swetlik, R. Dutta and B. D. Trapp (2018). "Alterations in CA1 hippocampal synapses in a mouse model of fragile X syndrome." Glia **66**(4): 789-800.

Jin, S. X., H. Higashimori, C. Schin, A. Tamashiro, Y. Men, M. S. R. Chiang, R. Jarvis, D. Cox, L. Feig and Y. Yang (2021). "Astroglial FMRP modulates synaptic signaling and behavior phenotypes in FXS mouse model." Glia **69**(3): 594-608.

Juczewski, K., H. von Richthofen, C. Bagni, T. Celikel, G. Fisone and P. Krieger (2016). "Somatosensory map expansion and altered processing of tactile inputs in a mouse model of fragile X syndrome." Neurobiol Dis **96**: 201-215.

Kalinowska, M., M. B. van der Lei, M. Kitiashvili, M. Mamcarz, M. M. Oliveira, F. Longo and E. Klann (2022). "Deletion of Fmr1 in parvalbumin-expressing neurons results in dysregulated translation and selective behavioral deficits associated with fragile X syndrome." Mol Autism **13**(1): 29.

Kramvis, I., H. D. Mansvelder, M. Loos and R. Meredith (2013). "Hyperactivity, perseveration and increased responding during attentional rule acquisition in the Fragile X mouse model." Front Behav Neurosci **7**: 172.

Lavedan, C., E. Grabczyk, K. Usdin and R. L. Nussbaum (1998). "Long uninterrupted CGG repeats within the first exon of the human FMR1 gene are not intrinsically unstable in transgenic mice." Genomics **50**(2): 229-240.

Lavedan, C. N., L. Garrett and R. L. Nussbaum (1997). "Trinucleotide repeats (CGG)22TGG(CGG)43TGG(CGG)21 from the fragile X gene remain stable in transgenic mice." Hum Genet **100**(3-4): 407-414.

Li, J., R. Y. Jiang, K. L. Arendt, Y. T. Hsu, S. R. Zhai and L. Chen (2020). "Defective memory engram reactivation underlies impaired fear memory recall in Fragile X syndrome." Elife **9**: e61882.

Li, J., M. R. Pelletier, J. L. Perez Velazquez and P. L. Carlen (2002). "Reduced cortical synaptic plasticity and GluR1 expression associated with fragile X mental retardation protein deficiency." Mol Cell Neurosci **19**(2): 138-151.

Liu, X., V. Kumar, N. P. Tsai and B. D. Auerbach (2021). "Hyperexcitability and Homeostasis in Fragile X Syndrome." Front Mol Neurosci **14**: 805929.

Lovelace, J. W., M. Rais, A. R. Palacios, X. S. Shuai, S. Bishay, O. Popa, P. S. Pirbhoy, D. K. Binder, D. L. Nelson, I. M. Ethell and K. A. Razak (2020). "Deletion of Fmr1 from Forebrain Excitatory Neurons Triggers Abnormal Cellular, EEG, and Behavioral Phenotypes in the Auditory Cortex of a Mouse Model of Fragile X Syndrome." Cereb Cortex **30**(3): 969-988.

Lu, J., M. Tjia, B. Mullen, B. Cao, K. Lukasiewicz, S. Shah-Morales, S. Weiser, L. P. Cameron, D. E. Olson, L. Chen and Y. Zuo (2021). "An analog of psychedelics

restores functional neural circuits disrupted by unpredictable stress." Mol Psychiatry **26**(11): 6237-6252.

Maddalena, A., C. S. Richards, M. J. McGinniss, A. Brothman, R. J. Desnick, R. E. Grier, B. Hirsch, P. Jacky, G. A. McDowell, B. Popovich, M. Watson and D. J. Wolff (2001). "Technical standards and guidelines for fragile X: the first of a series of disease-specific supplements to the Standards and Guidelines for Clinical Genetics Laboratories of the American College of Medical Genetics. Quality Assurance Subcommittee of the Laboratory Practice Committee." Genet Med **3**(3): 200-205.

Matsuzaki, M., G. C. Ellis-Davies, T. Nemoto, Y. Miyashita, M. Iino and H. Kasai (2001). "Dendritic spine geometry is critical for AMPA receptor expression in hippocampal CA1 pyramidal neurons." Nat Neurosci **4**(11): 1086-1092.

McKinney, B. C., A. W. Grossman, N. M. Elisseou and W. T. Greenough (2005). "Dendritic spine abnormalities in the occipital cortex of C57BL/6 Fmr1 knockout mice." Am J Med Genet B Neuropsychiatr Genet **136B**(1): 98-102.

Menon, L., S. A. Mader and M. R. Mihailescu (2008). "Fragile X mental retardation protein interactions with the microtubule associated protein 1B RNA." RNA **14**(8): 1644-1655.

Mientjes, E. J., I. Nieuwenhuizen, L. Kirkpatrick, T. Zu, M. Hoogeveen-Westerveld, L. Severijnen, M. Rife, R. Willemsen, D. L. Nelson and B. A. Oostra (2006). "The generation of a conditional Fmr1 knock out mouse model to study Fmrp function in vivo." Neurobiol Dis **21**(3): 549-555.

Monday, H. R., S. C. Kharod, Y. J. Yoon, R. H. Singer and P. E. Castillo (2022). "Presynaptic FMRP and local protein synthesis support structural and functional plasticity of glutamatergic axon terminals." Neuron **110**(16): 2588-2606 e2586.

Muddashetty, R. S., S. Kelic, C. Gross, M. Xu and G. J. Bassell (2007). "Dysregulated metabotropic glutamate receptor-dependent translation of AMPA receptor and postsynaptic density-95 mRNAs at synapses in a mouse model of fragile X syndrome." J Neurosci **27**(20): 5338-5348.

Musumeci, S. A., P. Bosco, G. Calabrese, C. Bakker, G. B. De Sarro, M. Elia, R. Ferri and B. A. Oostra (2000). "Audiogenic seizures susceptibility in transgenic mice with fragile X syndrome." Epilepsia **41**(1): 19-23.

Musumeci, S. A., R. J. Hagerman, R. Ferri, P. Bosco, B. Dalla Bernardina, C. A. Tassinari, G. B. De Sarro and M. Elia (1999). "Epilepsy and EEG findings in males with fragile X syndrome." Epilepsia **40**(8): 1092-1099.

Nagaoka, A., H. Takehara, A. Hayashi-Takagi, J. Noguchi, K. Ishii, F. Shirai, S. Yagishita, T. Akagi, T. Ichiki and H. Kasai (2016). "Abnormal intrinsic dynamics of dendritic spines in a fragile X syndrome mouse model in vivo." Sci Rep **6**: 26651.

Nimchinsky, E. A., A. M. Oberlander and K. Svoboda (2001). "Abnormal development of dendritic spines in FMR1 knock-out mice." J Neurosci **21**(14): 5139-5146.

Padmashri, R., B. C. Reiner, A. Suresh, E. Spartz and A. Dunaevsky (2013). "Altered structural and functional synaptic plasticity with motor skill learning in a mouse model of fragile X syndrome." J Neurosci **33**(50): 19715-19723.

Paluszkiewicz, S. M., J. L. Olmos-Serrano, J. G. Corbin and M. M. Huntsman (2011). "Impaired inhibitory control of cortical synchronization in fragile X syndrome." J Neurophysiol **106**(5): 2264-2272.

Pan, F., G. M. Aldridge, W. T. Greenough and W. B. Gan (2010). "Dendritic spine instability and insensitivity to modulation by sensory experience in a mouse model of fragile X syndrome." Proc Natl Acad Sci U S A **107**(41): 17768-17773.

Parrott, J. M., T. Oster and H. Y. Lee (2021). "Altered inflammatory response in FMRP-deficient microglia." iScience **24**(11): 103293.

Pfeiffer, B. E. and K. M. Huber (2007). "Fragile X mental retardation protein induces synapse loss through acute postsynaptic translational regulation." J Neurosci **27**(12): 3120-3130.

Pieretti, M., F. P. Zhang, Y. H. Fu, S. T. Warren, B. A. Oostra, C. T. Caskey and D. L. Nelson (1991). "Absence of expression of the FMR-1 gene in fragile X syndrome." Cell **66**(4): 817-822.

Pietropaolo, S., A. Guilleminot, B. Martin, F. R. D'Amato and W. E. Crusio (2011). "Genetic-background modulation of core and variable autistic-like symptoms in Fmr1 knock-out mice." PLoS One **6**(2): e17073.

Rais, M., D. K. Binder, K. A. Razak and I. M. Ethell (2018). "Sensory Processing Phenotypes in Fragile X Syndrome." ASN Neuro **10**: 1759091418801092.

Richter, J. D. and X. Zhao (2021). "The molecular biology of FMRP: new insights into fragile X syndrome." Nat Rev Neurosci **22**(4): 209-222.

Rodriguez, C. and N. Ji (2018). "Adaptive optical microscopy for neurobiology." Curr Opin Neurobiol **50**: 83-91.

Rudelli, R. D., W. T. Brown, K. Wisniewski, E. C. Jenkins, M. Laure-Kamionowska, F. Connell and H. M. Wisniewski (1985). "Adult fragile X syndrome. Clinico-neuropathologic findings." Acta Neuropathol **67**(3-4): 289-295.

Saneyoshi, T., D. A. Fortin and T. R. Soderling (2010). "Regulation of spine and synapse formation by activity-dependent intracellular signaling pathways." Curr Opin Neurobiol **20**(1): 108-115.

Scharkowski, F., M. Frotscher, D. Lutz, M. Korte and K. Michaelsen-Preusse (2018). "Altered Connectivity and Synapse Maturation of the Hippocampal Mossy Fiber Pathway in a Mouse Model of the Fragile X Syndrome." Cereb Cortex **28**(3): 852-867.

Sidhu, H., L. E. Dansie, P. W. Hickmott, D. W. Ethell and I. M. Ethell (2014). "Genetic removal of matrix metalloproteinase 9 rescues the symptoms of fragile X syndrome in a mouse model." J Neurosci **34**(30): 9867-9879.

Simhal, A. K., Y. Zuo, M. M. Perez, D. V. Madison, G. Sapiro and K. D. Micheva (2019). "Multifaceted Changes in Synaptic Composition and Astrocytic Involvement in a Mouse Model of Fragile X Syndrome." Sci Rep **9**(1): 13855.

Sinefeld, D., F. Xia, M. Wang, T. Wang, C. Wu, X. Yang, H. P. Paudel, D. G. Ouzounov, T. G. Bifano and C. Xu (2022). "Three-Photon Adaptive Optics for Mouse Brain Imaging." Front Neurosci **16**: 880859.

Soden, M. E. and L. Chen (2010). "Fragile X protein FMRP is required for homeostatic plasticity and regulation of synaptic strength by retinoic acid." J Neurosci **30**(50): 16910-16921.

Stein, I. S. and K. Zito (2019). "Dendritic Spine Elimination: Molecular Mechanisms and Implications." Neuroscientist **25**(1): 27-47.

The Dutch-Belgian Fragile X Consortium (1994). "Fmr1 knockout mice: a model to study fragile X mental retardation." Cell **78**(1): 23-33.

Till, S. M., L. S. Wijetunge, V. G. Seidel, E. Harlow, A. K. Wright, C. Bagni, A. Contractor, T. H. Gillingwater and P. C. Kind (2012). "Altered maturation of the primary somatosensory cortex in a mouse model of fragile X syndrome." Hum Mol Genet **21**(10): 2143-2156.

Turk, J. (2011). "Fragile X syndrome: lifespan developmental implications for those without as well as with intellectual disability." Curr Opin Psychiatry **24**(5): 387-397.

Verkerk, A. J., M. Pieretti, J. S. Sutcliffe, Y. H. Fu, D. P. Kuhl, A. Pizzuti, O. Reiner, S. Richards, M. F. Victoria, F. P. Zhang and et al. (1991). "Identification of a gene

(FMR-1) containing a CGG repeat coincident with a breakpoint cluster region exhibiting length variation in fragile X syndrome." Cell **65**(5): 905-914.

Vincent, A., D. Heitz, C. Petit, C. Kretz, I. Oberle and J. L. Mandel (1991). "Abnormal pattern detected in fragile-X patients by pulsed-field gel electrophoresis." Nature **349**(6310): 624-626.

Weiler, I. J., S. A. Irwin, A. Y. Klintsova, C. M. Spencer, A. D. Brazelton, K. Miyashiro, T. A. Comery, B. Patel, J. Eberwine and W. T. Greenough (1997). "Fragile X mental retardation protein is translated near synapses in response to neurotransmitter activation." Proc Natl Acad Sci U S A **94**(10): 5395-5400.

Wisniewski, K. E., S. M. Segan, C. M. Miezejeski, E. A. Sersen and R. D. Rudelli (1991). "The Fra(X) syndrome: neurological, electrophysiological, and neuropathological abnormalities." Am J Med Genet **38**(2-3): 476-480.

Xu, T., X. Yu, A. J. Perlik, W. F. Tobin, J. A. Zweig, K. Tennant, T. Jones and Y. Zuo (2009). "Rapid formation and selective stabilization of synapses for enduring motor memories." Nature **462**(7275): 915-919.

Zhang, Z., J. R. Gibson and K. M. Huber (2021). "Experience-dependent weakening of callosal synaptic connections in the absence of postsynaptic FMRP." Elife **10**: e71555.